In-plane Behavior of Reinforced Concrete Shear Walls with poor Flexural Reinforcement, Strengthened with FRP strips

Mateo Pulido Ulloa

Escuela Colombiana de Ingeniería Julio Garavito

Master's Degree in Civil Engineering

Bogotá, D.C., Colombia

2021

In-plane Behavior of Reinforced Concrete Shear Walls with poor Flexural Reinforcement, Strengthened with FRP strips

A thesis submitted in partial fulfillment of the requirements for the degree of master's in civil engineering with emphasis on Structural Engineering

Nancy Torres Castellanos, PhD.

Advisor

Fancisco José de Caso y Basalo, PhD.

Co-Advisor

Bogotá, D.C., Colombia

2021

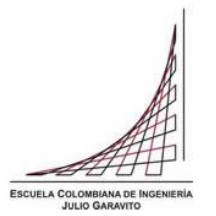

Master´s Thesis entitled ¨In-plane Behavior of Reinforced Concrete Shear Walls with poor Flexural Reinforcement, Strengthened with FRP sheets ¨, submitted by Mateo Pulido Ulloa, fulfill the requirements established to qualify for the Master´s degree in Civil Engineering with an emphasis on Structural Engineering

Advisor:

Nancy Torres Castellanos, M. Sc., PhD.

Co-advisor:

Francisco José De Caso y Basalo, M.Sc.,PhD

Approved:

Carlos Eugenio Palomino Arias, I.C., M.Sc., P.E.

Jury 1

Ismael Santana Santana, I.C., M.Sc.

Jury 2

Bogotá D.C., July 28th, 2021 (Approval date)

ACKNOWLEDGMENTS

To my family and friends, for their unconditional support and blind trust in my capacities.

To Escuela Colombiana de Ingeniería Julio Garavito, because it has been, and will always be, my home. Special mention deserves all the staff of the structures and materials laboratory for doing everything possible to help me.

To Dr. Nancy Torres Castellanos for always trusting me and giving me the great opportunity to work and learn by her side, for supporting me and demanding more of me every day. None of this would be possible without her invaluable support.

To my mother, the person who has given everything in her life to see me grow. She is the engine that works tirelessly to see me succeed…

Mom, I want you to know that all my achievements are, and will be, yours.

Abstract

There is a large amount of thin wall buildings in the country that have been constructed on inadequate designs, have extended their service life or have had changes in the type of use in structures, among other factors. Under these circumstances, these constructions have a high degree of vulnerability. This, added to the important seismic threat present in cities with the highest number of inhabitants, results in a risk of significant damage to buildings, which could even collapse. This research tested a system that could allow to repair or rehabilitate the walls of these buildings, using non-invasive systems like Fiber-reinforced polymers (FRP).

FRP are an emerging repair or rehabilitation alternative that in recent years has become very popular. External reinforcement with FRP bands improves the bending and shear capacities of existing structures. This reinforcement system is even suitable for repairing structures with insufficient or degraded capacities after its elements had been subjected to seismic stresses.

This document presents the results obtained in a research project that evaluated the behavior of reinforced concrete walls with vertical reinforcement deficiencies. The walls were externally reinforced with different types of FRP bands to improve their flexural capacities. 6 specimens of 0.1 x 1.5 x 5 m (4 x 59 x 197 in) were analyzed: 4 with concrete with low compressive strength and 2 with concrete with high compressive strength. The latter were externally reinforced with two types of carbon fibers (CFRP): one with a high elastic modulus (CHM) and another with a lower elastic modulus (CHS) and a type of fiberglass (GHS).

The failure mode, hysterical response, stiffness degradation, ductility and energy dissipation capacity were evaluated. The bending capacities of the walls reinforced with each of the FRP bands showed an important improvement. Finally, the design methodology and calculation of theoretical capacities for this type of reinforcement, present in document ACI 440.2R-17, was corroborated. Thus, it was found an adequate correlation between the experimental results and the capacities theoretically calculated.

Resumen

El gran número de edificios de muros delgados construidos en el país, junto a diseños de muros de concreto inadecuados, cambios de tipo de uso en estructuras entre otros factores, representan un alto grado de vulnerabilidad de las construcciones y esto sumado a la importante amenaza sísmica presente en las ciudades con mayor número de habitantes da como resultado un riesgo de daño importante de las edificaciones e incluso de colapso. Los polímeros reforzados con fibra (FRP) son una alternativa emergente de reparación o rehabilitación que en los últimos años ha tenido gran auge. El reforzamiento externo con bandas de FRP mejora las capacidades por flexión y por corte de muros existentes o incluso este sistema de reforzamiento es apto para reparaciones de estructuras con capacidades degradadas al haber sido sometidos los elementos a solicitaciones sísmicas.

En el presente documento se exponen los resultados obtenidos en un proyecto de investigación donde se evaluó el comportamiento de muros de concreto reforzado con deficiencias de refuerzo vertical, reforzados externamente con distintos tipos de bandas de FRP con el fin de mejorar sus capacidades a flexión. Se analizaron 6 especímenes de 0.1 x 1.5 x 5 m (4 x 59 x 197 in); 4 con concreto de baja resistencia a la compresión y 2 especímenes con concreto de alta resistencia a la compresión, reforzados externamente con dos tipos de fibras de carbono (CFRP), una de alto módulo elástico (CHM) y otra de menor módulo elástico (CHS) y un tipo de fibra de vidrio (GHS).

Se evaluó el modo de falla, la respuesta histerética, la degradación de la rigidez, la ductilidad y la capacidad de disipación de energía, encontrando una mejora importante en las capacidades por flexión de los muros reforzados con cada una de las bandas de FRP. Finalmente se corroboró la metodología de diseño y cálculo de capacidades teóricas para este tipo de reforzamiento presente en el documento ACI 440.2R-17, encontrando una adecuada correlación entre los resultados experimentales y las capacidades calculadas teóricamente.

CONTENT

List of Figures

List of Tables

Introduction

Colombia is in a complex tectonic site, due to its position on the convergence of three great tectonic plates: the Nazca plate, the South American plate, and the Caribbean plate. The main seismotectonic accident is the subduction zone of the Nazca plate under the South American plate, on the Pacific coast (García, 1998). This tectonic movement, present on the east coast of the South American continent, is the main source of seismic threat for Colombia (INGEOMINAS, 2005). However, apart from the subduction zone, there are other numerous active geological faults in the Colombian territory (García, 1998).

The presence of these geological accidents implies that Colombia presents an important seismic threat in some regions, mainly the central, western, and northwestern ones. For this reason, a seismic threat study was carried out at a national level, which divided the country in three large areas, depending on the probability of occurrence of major earthquakes in each city. The categories of those areas were low, intermediate, and high seismic hazard zone. The cities with the highest number of habitants, such as Bogotá, Medellín and Cali (Portafolio, 2019), are located in areas of considerable seismic threat. According to the seismic hazard study carried out by the Colombian Association of Seismic Engineering (AIS), about 40% of Colombians live in high seismic hazard areas, and 47% in intermediate seismic hazard areas. In other words, 87% of the Colombian population is under a considerable level of seismic risk (Correal, 2016). For this reason, it is necessary to guarantee that buildings throughout the country have adequate behavior in the face of seismic stresses and, thus, protect the life, honor and property of citizens.

The wall system is one of the structural systems most used in recent years in the country, due to its low cost in construction, its efficiency in delimiting architectural spaces, and its effectiveness in limiting damage before high intensity seismic solicitations, due to the rigidity of regular thickness walls. However, the tendency of designer and builder engineers to seek optimizations has resulted in a significant reduction in wall thicknesses, leading to very slender walls.

The slender wall system has demonstrated adequate seismic performance in low-rise buildings, up to three stories high. However, in recent years there has been a direct extrapolation of the behavior of thin walls in low-rise buildings to high-rise buildings, which has been shown to not perform well (Colombian Earthquake Engineering Research Network (CEER), 2018).

In current practice, thin walls, with thicknesses of up to eight centimeters, are used in buildings of even more than 12 stories high (CEER, 2018). Their longitudinal reinforcement and shear reinforcement typically consist of electro-welded meshes made up of wires with limited ductility (Julian Carrillo et al., 2019) or steel bars with low diameters, placed forming a single reinforcing grid, without confinement, since the low thickness of the wall does not guarantee adequate separation and/or coatings when two meshes are placed. Additionally, in some cases it has been found that they do not have edge elements. And, according to experimental investigations carried out, this type of walls have shown reduced ductility (Julián Carrillo et al., 2016).

Taking this into account, the aim of this project consists in assessing the bending behavior of thin reinforced concrete walls that are subject to in-plane lateral load and strengthened with different types of fibers reinforced polymers —from now on, FRP—. Hopefully, the results of this research could help in bringing awareness on the importance of well-thought design, construction, and reinforcement of high-rise buildings. The methodology used to carry out this research project is made up of two parts: the first consisted of a bibliographic search and the second in the execution of an experimental program.

The document consists of 6 chapters.

Chapter 1 presents a general review of the problem presented by reinforced concrete walls, followed by overview of the strengthening whit FRP. Finally, a review of the design requirements for wall reinforcement provided in the ACI 440.2R-17 code is carried out.

Chapter 2 presents the main contributions made by different authors in relation to the behavior of concrete walls reinforced in flexion with FRP, when they are subjected to lateral loads in the plane.

Chapter 3 sets out the general objective and the specific objectives of the research that allowed the development of each of the proposed variables to be carried out successfully.

With the development of the state of the art, later in chapter 4, comes a description of the physical and mechanical properties of the materials used in the present investigation. The variables of the experimental study are also presented, as well as an individual characterization of the test specimens and their construction and reinforcement process.

The results obtained from the experimental program are analyzed in chapter 5. The result of the cyclic tests of each of the test specimens is presented together with the hysteresis curves from the displacements measured in the plane and the load readings reported by the dynamic actuator. With these curves, the level of ductility reached and the maximum values of the resistant capacity of the specimens were calculated. Graphs of degradation of lateral stiffness were generated to evaluate the behavior of the walls as the load cycles progress.

Chapter 6 presents the conclusions obtained from the development of the research and recommendations for future research related to the subject under study. Finally, the bibliography used is listed.

1. THEORETICAL FRAMEWORK

1.1. Overview

This chapter presents a general review of the problem presented by reinforced concrete walls, followed by overview of the strengthening whit FRP. Finally, a review of the design requirements for wall reinforcement provided in the ACI 440.2R-17 code is carried out.

1.2. Problematic

The thin reinforced concrete walls system —from now on, RCWS— has demonstrated a good behavior in buildings up to three floors (low-rise buildings). But, in a recent study, the Colombian Earthquake Engineering Research Network (CEER, 2018) found that buildings up to 12 stories were constructed with this system, as a result of direct extrapolation of the behavior of thin reinforced concrete walls in low-rise buildings to taller buildings.

Following Qazi *et al.* (2013), the previously mentioned finding could constitute a major risk, since slender walls are sensitive to bending. This could lead to failure either by concrete toe crushing, or by yielding of vertical reinforcement, or, even, by a combination of both. Shear slipping of wall occurs in some cases. Hiotakis *et al.* (2004) observed common deficiencies in old shear wall structures, such as insufficient flexural capacity and ductility due to insufficient flexural reinforcement. Besides, Panneton *et al.* (2006) have highlighted that shear walls that were constructed in conformity to older design codes might currently be considered seismically deficient. This derives from the fact that modern codes consider that shear walls may experience higher demands at upper stories, as an effect of the higher vibration modes.

The Chilean (2010) and New Zealand (2011) earthquakes made these deficiencies evident. Buildings with thin and slender reinforced concrete walls —from now on, RCW— presented higher damage than what was expected, according to design earthquake (CEER, 2018). In Chile, San Bartolomé *et al.* (2011) registered, among others, bending failures in the reinforced concrete thin walls —from now on, RCTW—, as shown in Figure 1-1.

Figure 1-1-Flexural RC walls failure during Chilean (2010) earthquake.
Source: adapted from San Bartolomé *et al.* (2011)

These recent earthquake experiences and investigations concluded that RCTW systems are not suitable for tall buildings. This has led CEER (2018) to consider that the current design requirements set forth in the Colombian Seismic Resistance Code —from now on, NSR-10, following its initials in Spanish— are not sufficient to guarantee good structural behavior. This is because slender walls, with high axial load ratio and lack of edge elements, have low displacement capacity, different types of brittle failure, and low energy dissipation capacity. On this subject, Blandón *et al.* (2015) found that, when the slender walls reach a drift of 1%, they lose about 80% of their initial lateral stiffness, which represents a considerable degradation. San Bartolomé et al., (2007) reached similar results, where they found that these thin walls reinforced with a single electro-welded mesh present a limited energy dissipation capacity.

Given these findings, the CEER (2018) has proposed to define the slender RCWS as an independent structural system, with a coefficient of energy dissipation capacity (R_0) lower than that established for conventional walls, in title A of the NSR-10, as can be seen in Table 1.1. That is the same coefficient value that San Bartolomé et al., (2007) determined in their study for thin RCWS.

Table 1.1- Proposed modification of the CEER to Table A.3-1 of the NSR-10.

SEISMIC RESISTANCE SYSTEM	VALUE Ro	Seismic Hazard Zone						Source
		high		Intermediate		Low		
		Permitted use	Max height	Permitted use	Max height	Permitted use	Max height	
RC walls with special energy dissipation capacity (DES)	5	YES	50 m	YES	Unlimited	YES	Unlimited	(NSR-10, 2012)
RC walls with moderate energy dissipation capacity (DMO)	4	Not allowed		YES	50 m	YES	Unlimited	(NSR-10, 2012)
Thin RC walls with limited energy dissipation capacity	3	YES	12 m	YES	20 m	YES	24 m	(CEER, 2018)

Source: adapted from CEER (2018)

These results indicate that the coefficients of energy dissipation capacity, used since 2010 for most buildings with a thin wall system, were possibly overestimated. As a result, these constructions will present low seismic behavior.

1.3. Overview of external reinforcement with FRP sheets

Different methods have been developed for seismic strengthening or retrofit to reduce the risk of collapsing in old deficient shear buildings. It is necessary that these methods neither imply massive evictions nor entail considerable costs for its inhabitants. Taking these premises into consideration, the external reinforcement with FRP fabrics is proposed as an option. FRP have advantages over traditional reinforcement systems, since they do not require demolition, being a non-invasive technique. As result there is less production of dust, noise, and debris.

Some traditional methods such as increase the thickness of the wall face is efficient in improving or recovering their gravitational load capacities but is not effective in increasing the lateral stiffness of the structure. The lateral stiffness of the structure could increase using another reinforcement method: the addition of reinforcing bars to the walls. Nonetheless, this method requires major architectural changes that could lead to a significant redistribution of loads in the structure, leading to a reconfiguration of the ways in which seismic loads are distributed within the structure (Hiotakis et al., 2004).

FRP are an emerging structural repair or rehabilitation alternative, due to their lightness, lack of corrosion, high tensile strengths and elastic modulus, high resistance to insect and fungal growth, high resistance to chemical attack, low thermal transmissibility and ease of installation (Siddika et al., 2020). The material consists of synthetic epoxy resin and fiber (Vega, 2015). Epoxy resin is generally used to adhere bands to the element to be reinforced. Meanwhile, carbon (CFRP), glass

(GFRP) and/or aramid (AFRP) fibers could be used. Figure 1-2 compares the stress-strain behaviors of different FRP materials with that of mild steel, which is clear evidence of the high strength of FRPs relative to those of other conventional materials.

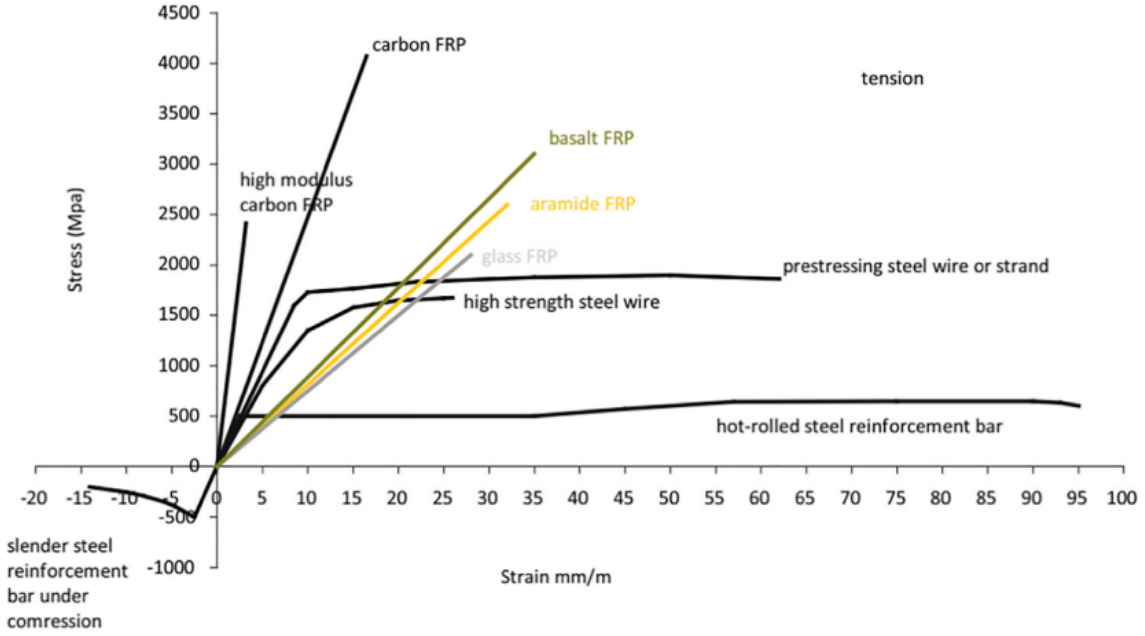

Figure 1-2- comparison of typical FRP materials with mild steel.
Source: Siddika et al., (2020)

Most of them present linear elastic behavior up to failure as Figure 1-2 shows. Carbon fibers generally have higher elastic modulus and ultimate tensile stress than other types of fibers, while glass fibers have lower elastic modulus and lower ultimate tensile strengths but higher ultimate strain, therefore these fibers have a higher deformation capacity. (Rousakis, 2014)

To increase the flexural strength an externally bonded FRP sheet aligned along the tension face of a concrete structure is the most common and provide excellent performance under bending, whereas the fibers in FRP sheets need to be arranged along the length of the member (Teng et al., 2003).

The common failure mode of FRP-strengthened RC structures under bending is debonding, which reduces the effectiveness of the strengthening. Debonding is an important failure mode as it prevents the full ultimate flexural capacity of the element from being achieved. The most commonly reported debonding mode is the separation of the concrete cover together with the plate which propagates from the end of the plate, due to high interfacial stresses at the plate end (Teng et al., 2003). The Figure 1-3 Shows the process of debonding propagation in a slab with FRP strengthened.

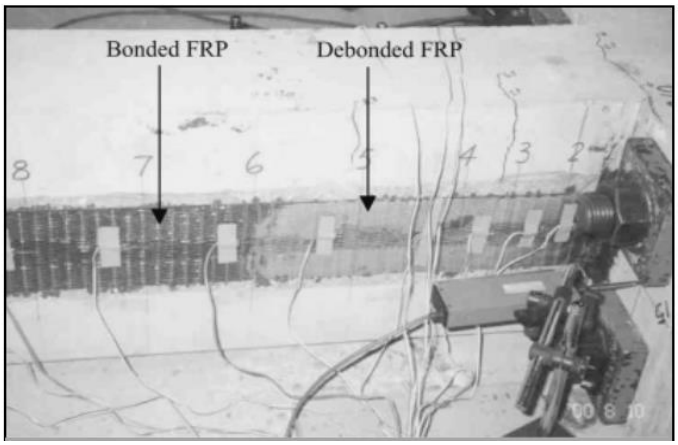

Figure 1-3- FRP-strengthened RC cantilever slabs in the process of debonding propagation
Source: (Teng et al., 2003)

To guarantee an optimal adhesion between the FRP system and the concrete, it must be ensured that the concrete surfaces to which the FRP system is to be applied should be freshly exposed and free of loose or unsound materials. Obstructions and embedded objects may need to be removed before installing the FRP system. Surface preparation can be accomplished using abrasive or water-blasting techniques. All laitance, dust, dirt, oil, curing compound, existing coatings, and any other matter that could interfere with the bond of the FRP system to the concrete should be removed. Bug holes and other small surface voids should be completely exposed during surface profiling. After the profiling operations are completed, the surface should be cleaned and protected before FRP installation so that no materials that can interfere with bond are redeposited on the surface. The concrete surface should be prepared to a surface not less than CSP3, as defined by ICRI 310.2R.(ACI 440.2R, 2017)

1.4. ACI 440.2R-17 specifications for flexural strengthening with FRP of RC walls

ACI 440.2R-17, in chapter 13.7, presents design guidelines for the seismic strengthening of reinforced concrete walls. To increase the shear capacity is necessary to apply horizontal FRP fabrics along the height of the walls, and to increase the in-plane flexural capacity is necessary applying vertical FRP bands at the ends or boundaries on one or both sides of walls (ACI 440.2R, 2017). These suggestions are based on experimental programs developed by Lombard *et al.* (2000) and Hiotakis *et al.* (2004).

To avoid a brittle shear failure, it is important to evaluate and compare the flexural strength with the shear strength for the walls reinforced with FRP for flexure.

The flexural strength of a section depends on the controlling failure mode. The most common failure modes are: crushing of the concrete in compression before yielding of the reinforcing steel; yielding of the steel in tension followed by rupture of the FRP laminate; yielding of the steel in tension followed by concrete crushing; concrete cover delamination; and debonding of the FRP from the concrete substrate. The concrete crushing occurs when the compressive strain reaches its maximum (ε_{cu}=0.003). The rupture of the FRP occurs when the strain in the FRP reaches its rupture strain (ε_{fu}).

The debonding of the FRP occurs when the strain in FRP reaches the strain at which debonding may occur (ε_{fd}), as defined in Equation 1, where *n* is de FRP layer number (ACI 440.2R, 2017).

$$\varepsilon_{fd} = 0.41\sqrt{\frac{f'c}{n \cdot E_f \cdot t_f}} \leq 0.9 \cdot \varepsilon_{fu} \qquad (S.I)$$

Equation 1
Source: (ACI 440.2R, 2017)

The flexural capacity of the strengthening wall must be calculated assuming a strain compatibility between concrete, FRP bands and the reinforcing steel bars, as well as the assumption that plane sections remain plane. The Figure 1-4 shows the main variables required for design.

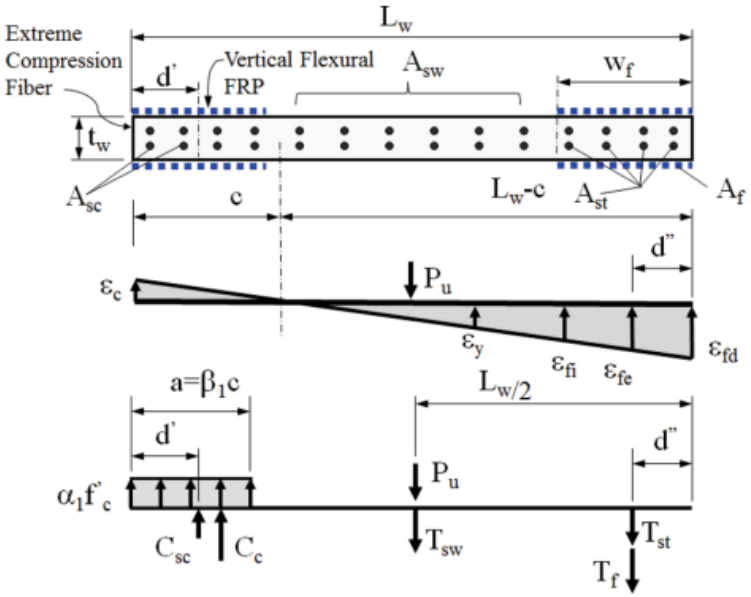

Figure 1-4- FRP reinforcement for flexural strengthening.
Source: (ACI 440.2R, 2017)

Flexural design involves iteration to achieve equilibrium across the section. It is necessary first to assume a depth of the neutral axis c. Once the depth of the neutral axis is assumed, concrete strain limits must be verified assuming that the strain at which debonding of the FRP may occur (ε_{fd}) is presented at the end of the wall as Figure 1-4 shows. The concrete compressive strains ε_c should be limited by Equation 2.

$$\varepsilon_c = \varepsilon_{fd} \cdot \left(\frac{c}{L_w}\right) \leq \varepsilon_{cu}$$

Equation 2
Source: (ACI 440.2R, 2017)

Where ε_{cu} should be limited to the following values shown in Equation 3:

$$\varepsilon_{cu} \leq 0.010 \ \ for\ confined\ concrete\ at\ bundaries$$
$$\varepsilon_{cu} \leq 0.003 \ \ for\ unconfined\ concrete\ at\ bundaries$$

Equation 3
Source: (ACI 440.2R, 2017)

Next, the depth of the neutral axis must be recalculated with Equation 4. For this, it is necessary to calculate the forces in the materials, corresponding to the strain of each one.

$$c = \frac{a}{0.85} \qquad a = \frac{T_{sw} + T_f}{0.85 \cdot f'c \cdot t_w}$$

Equation 4
Source: (ACI 440.2R, 2017)

Were T_{sw} is the total force of bars in tension and T_f is the tensile force of the FRP corresponding to the strain at the centroid of the FRP area (ε_{feCG}). The calculations of the strain in flexural steel reinforcement (ε_s) and the strain at centroid of FRP area (ε_{feCG}) are made considering a linear deformation of the section as the Figure 1-4 shows.

An iterative process must be carried out, varying the depth of the neutral axis initially assumed until obtaining the same depth of the neutral axis assumed and finally calculated.

Finally, the strains, lever arms and force components in concrete, FRP and reinforcing steel will be calculated to determine the moment capacity of the wall. Annex B presents a detailed design example.

It is important to guarantee the continuity of the load path of the walls, for this a correct anchorage of the flexural reinforcement bands must be guaranteed both in the foundations and in the slabs. The ACI 440.2R document provides two conceptual methods of bending reinforcement anchors, however any anchoring method used in the field should be properly evaluated. The Figure 1-5 shows conceptual anchorage methods proposed by the ACI.

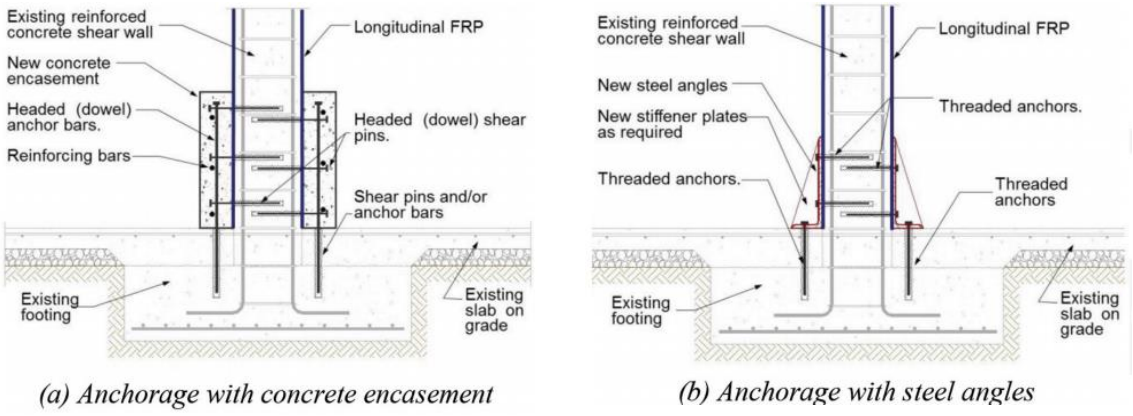

Figure 1-5- Conceptual anchorage methods for strengthened shear wall.
Source: (ACI 440.2R, 2017)

The anchoring of the vertical reinforcement fibers is necessary to guarantee a correct behavior of the flexural reinforcement system with FRP bands.

2. STATE OF THE ART

2.1. Overview

This chapter presents an overview of existing knowledge on FRP systems for the flexural strengthening of reinforced concrete walls. Starting with a review of studies carried out on the reinforcement with FRP of reinforced concrete walls with longitudinal reinforcement deficiencies, followed by a review of studies carried out on the behavior of different types of reinforcing fibers in concrete walls. Finally, a review of studies carried out on the adherence of FRP sheets on the concrete surface.

2.2. Flexural strengthening of RC walls with FRP

Trumialan *et al.* (2009) found that external reinforcement with FRP sheets improves the bending and shear capacities of existing structures. The authors stated that this reinforcement system is suitable for repairing structures with degraded capacities like those whose elements have been exposed to seismic stresses.

Although the abundance of publications around the benefits of reinforcement of structural elements with FRP, few authors have carried out studies on the performance of externally reinforced walls with FRP bands. Lombard *et al.* (2000) and Hiotakis *et al.* (2004) have analyzed the latter topic.

Their studies have shown that the use of FRP as a reinforcement alternative is an effective option and that it considerably improves the capacities of the walls under bending stresses. These teams conducted tests to improve the bending capacities of RCW using FRP bands as a strengthening method. They chose to place the fibers vertically to test reinforcement in two types of walls: the first type were walls with an initial reinforcement with FRP, and the second one were walls without initial external reinforcement that were subsequently repaired. In this way, the fibers would contribute to increase the bending capacity of the walls in a similar way in which the longitudinal reinforcing steel bars do. Separately, though concordantly, they found that this orientation of the fibers increases the lateral stiffness and yield capacity of the wall. In deteriorated concrete walls, they found that FRP bands could increase ultimate capacity, surpassing the results obtained during their first tests without external reinforcement, as well as help recover initial stiffness. These reinforcements could increase walls' ultimate bending capacity to even exceed the one originally shown during tests.

Further studies include that of Cruz-Noguez *et al.* (2015), who conducted tests of strengthening RC walls. The research evaluated nine (9) specimens, including: walls initially conceived with external FRP reinforcement; walls extensively repaired with FRP bands after damage; and control walls without FRP. The external reinforcement of the walls consisted of FRP bands that completely covered the faces of the wall. On all the walls, the fibers were put in a vertical direction. And, in those cases in which the shear capacity was exceeded, by increasing the bending capacities of the walls, also were added horizontal fibers, to prevent a bearing shear failure. The strengthening specimens are shown in Figure 2-1.

Figure 2-1- Tests for specimens' strengthening with FRP bands on both sides of the wall
Source: Cruz-Noguez et al., 2015

The RC walls were tested with quasi-static load cycles applied by a hydraulic actuator at the top of the specimens, as shown in Figure 2-2. In first instance, loads were applied until reaching the theoretical yielding load. Posteriorly, researchers increased the load, according to displacement-controlled protocol, up to failure.

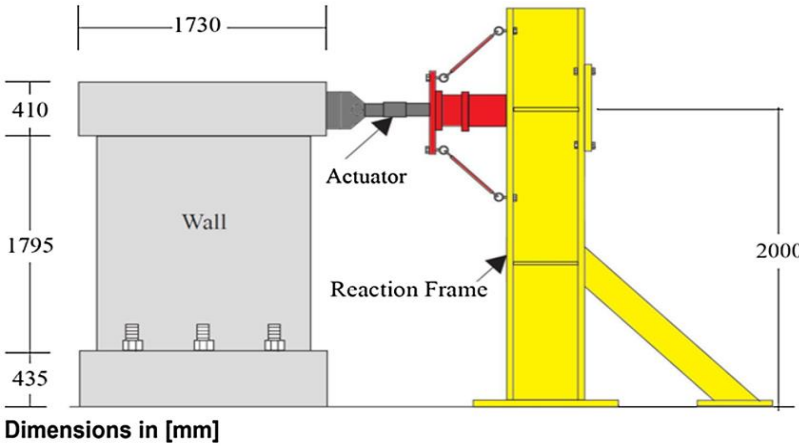

Figure 2-2- Load Test set-up implemented by Cruz-Noguez et al. (2015).
Source: Cruz-Noguez et al., 2015

Cruz-Noguez *et al.* (2015) found that in the repaired specimens, the FRP reinforcement system showed a recovery of most of the initial stiffness of the wall and increased its maximum flexural capacity. For the case of the specimens reinforced with FRP, higher stiffnesses and ultimate capacities were obtained, in comparison to the performance of control walls.

El-Sokkary & Galal (2013) carried out an investigation to determine the behavior of RCW strengthening with two different retrofit schemes of CFRP bands, when exposed to lateral loads. Three specimens, with deficiencies in flexural reinforcement, were tested under cyclic loading leading up to failure. The tested walls represent a control wall (without FRP) and two FRP-retrofitted walls using two different schemes with the main target to increase their flexural capacity and, therefore, enhance them to resist higher seismic demands.

The first retrofit scheme consisted in covering the ends of both faces of the walls with two vertical CFRP sheets with 20 cm of width, combined with the overlay of the entirety of the walls' faces with horizontal FRP bands, to increase the shear capacity of the wall and avoid a shear brittle failure mode before reaching its increased flexural capacity. In the other retrofit scheme, the shear and flexural capacities were increased by placing diagonal FRP sheets on each face of the wall. The diagonal bands produce an inclined force that can be decomposed into vertical and horizontal components. Figure 2-3 shows the two retrofit schemes.

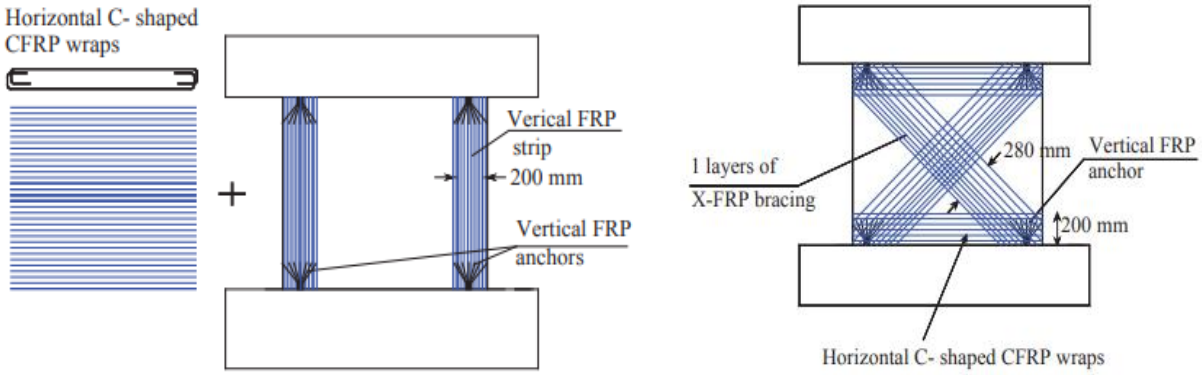

(a) Vertical and horizontal FRP strips retrofit scheme. **(b) Diagonal FRP strips retrofit scheme.**

Figure 2-3-El-Sokkary & Galal, 2013 test retrofit schemes
Source: El-Sokkary & Galal, 2013

The results showed that the first scheme, with vertical bands at the ends, increased the lateral capacities at yield of the wall by 46%, with respect to the control. The second scheme, emulating an X shape, only helped increased lateral capacities by 19% in contrast to the control. The first scheme produced further better results in terms of flexural capacity, presenting an 80% increase, compared to 50% of the "X" scheme.

However, the experimental capacity of the wall with vertical sheets was higher than theorical expected capacity. Therefore, there were premature failures of the anchoring systems that transmitted the stresses of the vertical bands to the bottom beam of the wall. Due to this premature failure, it was not possible to determine the real flexural capacity that this retrofit scheme adds to the walls.

Shen et al., (2017) carried out an investigation to determine the behavior of RCW strengthening with different retrofit schemes of BFRP sheets, the test specimens consisted of cantilever walls subjected to cyclic loads. Five specimen's whit different reinforced schemes were constructed. The results

showed that the strengthening whit lateral strips (SHW4 according to the Figure 2-4) presents the best performances for the improvement of ductility and load carrying capacity. The Figure 2-4 shows the tested strengthening schemes.

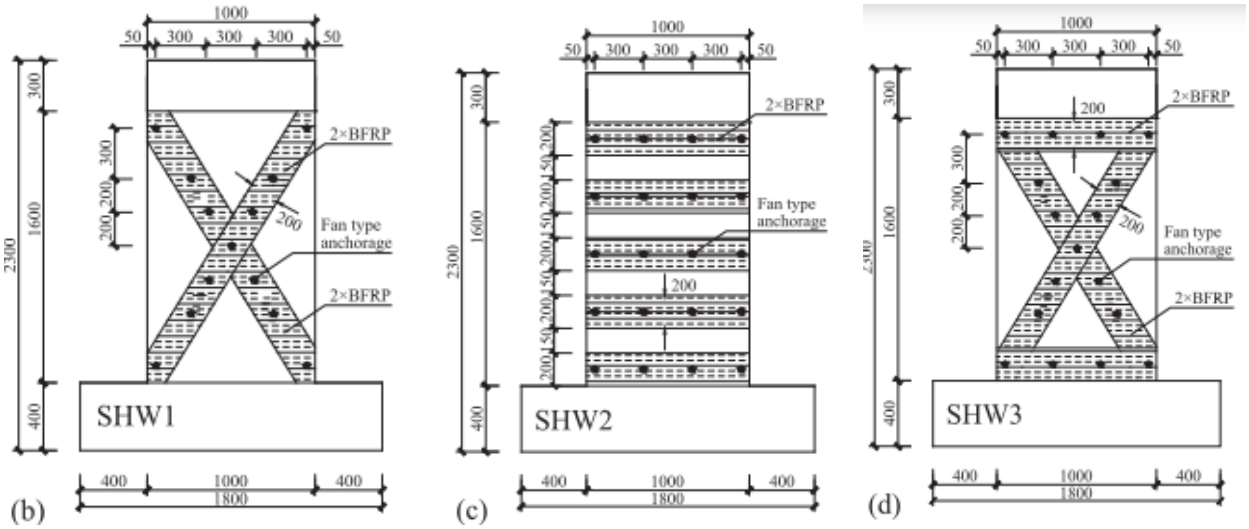

(a) SHW1 specimen. **(b) SHW2 specimen.** **(c) SHW3 specimen**

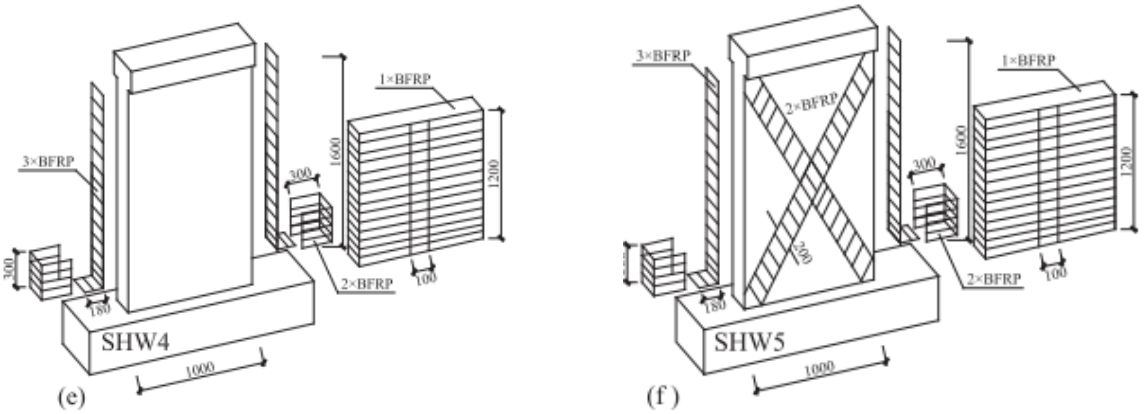

(d) SHW4 schemen. **(e) SHW5 scheme.**

Figure 2-4-Shen et al., (2017) test retrofit schemes
Source: Shen et al., (2017)

2.3. Flexural strengthening with different FRP types

Sheikh et al. (2002) carried out an investigation to compare the behavior of full-scale walls repaired with GFRP and CFRP. The experimental program included testing of three wall specimen. The wall specimens were 0.250 m (9.8 in) thick, 1.2 m (47 in) wide, and 1.2 m (47 in) long. Two-line loads were applied to the specimen out of plane to produce flexural cracking in the central third. The loading and support conditions for wall specimens are shown in Figure 2-5.

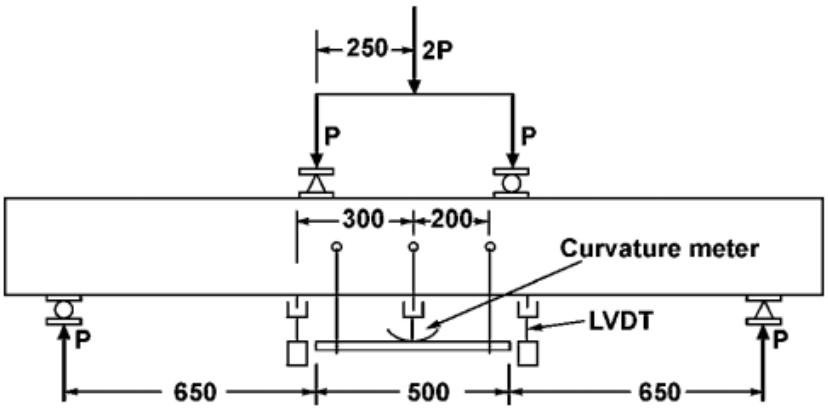

Figure 2-5- Loading and support conditions for wall specimens
Source: Sheikh et al., 2002

The specimens had flexural reinforcement deficiencies to achieve flexural failure. Three strips of fabric, approximately 600 mm (24 in) wide, were used as shown in Figure 2-6 to increase the out of the plane bending capacity of the wall.

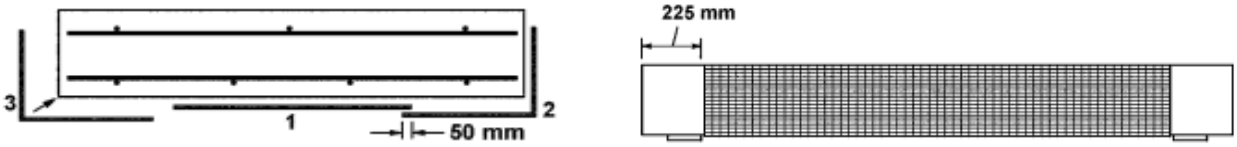

(c) Cross-Section **(d) Elevation showing zone of FRP-repair**

Figure 2-6- Application of FRP on wall specimens
Source: Sheikh et al., 2002

The response of both the repaired specimens was reasonably ductile and resulted in a large energy dissipation, though not as ductile as the control specimen. The GFRP-repaired specimen showed higher ductility than the CFRP-repaired specimen. Therefore, if higher ductility, rather than the strength, is desired, a lesser amount of FRP reinforcement should be applied. It was also found that both carbon and glass composites provided significant enhancement (more than 148%) in flexural strength of the wall specimens.

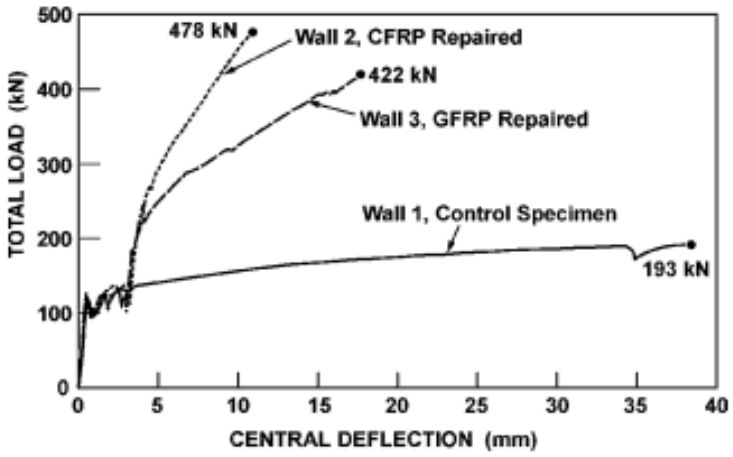

Figure 2-7- Load-deflection behavior of wall specimens.
Source: Sheikh et al., 2002

Di Luccio et al., (2017) carried out a study to compare the behavior of flexural strengthening RC walls whit different FRP types. Three specimens were tested under cyclic in-plane loading leading up to failure. The test specimens consisted of a control wall, without any reinforcement, two walls with external CFRP reinforcement (SLR4 and SLR6), two walls with external reinforcement of Flex FRP -for now FFRP- (FRSL1 and FRSL2) and a last wall with mixed external reinforcement composed of FFRP and GFRP sheets (FRSL-3). The test retrofit schemes are shown in the Figure 2-8.

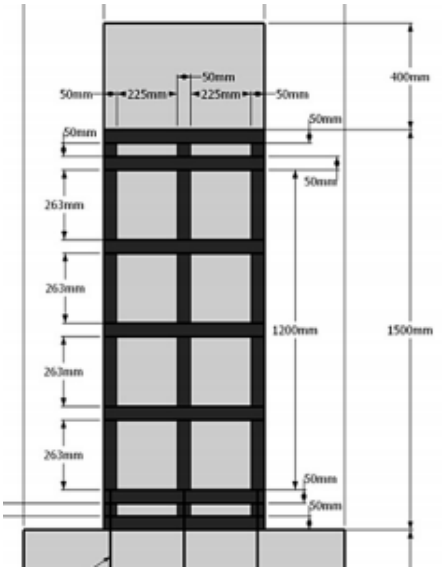

(a) SLR4 specimen with CFRP strengthening.

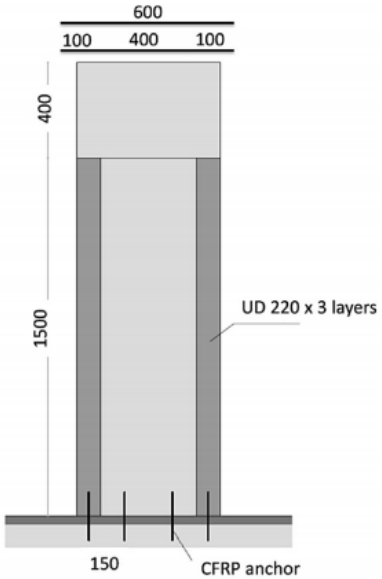

(b) SLR6 specimen with CFRP strengthening.

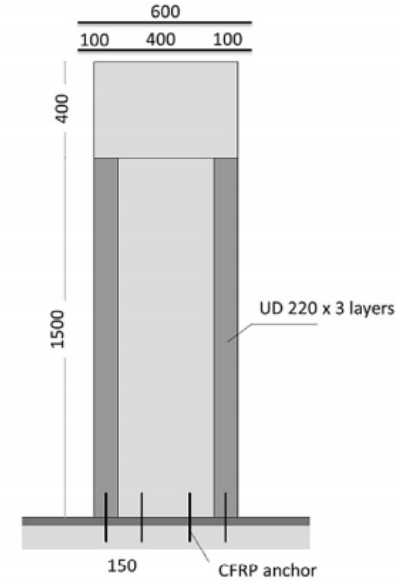

(c) FRSL 1 specimen whit FFRP strengthening.

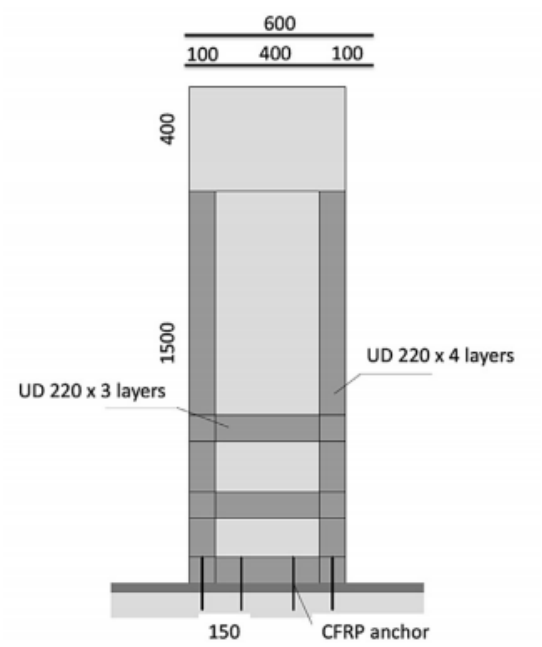

(d) FRSL 2 specimen whit FFRP strengthening.

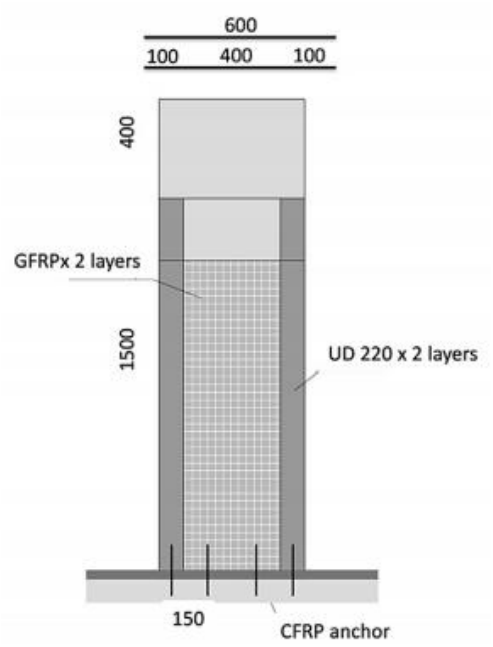

(e) FRSL 3 specimen whit FFRP and GFRP strengthening.

Figure 2-8-Di Luccio et al., (2017) test retrofit schemes

Source: Di Luccio et al., (2017)

The RC walls were tested with load cycles applied by a hydraulic actuator at the top beam of the specimens. To understand the results, it is important to note that FFRP has lower ultimate resistance than CFRP and GFRP. But it has a higher elastic modulus than GFRP and a lower modulus than CFRP.

The results show that the specimens reinforced with both FFRP and CFRP show an increase in resistance up to 150% compared to the control wall. Additionally, the CFRP was the reinforcement system that presented the longest delay in the process of deterioration of the stiffness of the walls. However, it is found that glass fibers (GFRP) increase the energy dissipation capacity of the wall, an important property in seismic reinforcement.

2.4. Bond behavior between FRP sheets and Concrete

Recently, many studies have been undertaken to understand the bond behavior between concrete and FRP sheets. Nakaba et al., (2001) conduced a double-face shear type bond test to examine the bond behavior between FRP sheets and concrete, the test variables were the types of fiber and concrete compressive strength. The test specimens consisted of a concrete prism (100 x 100 x 600 mm) (4 x 4 x 24 in) cracked at the center using a hammer after the reinforcing with FRP sheets, which means that the two prisms were connected only through the FRP. The sheets were bonded at two opposite sides of the specimen and one of the sides of the specimen was reinforced with a confinement FRP allowing the occurrence of delamination of the FRP only on opposite side as the Figure 2-9 shows.

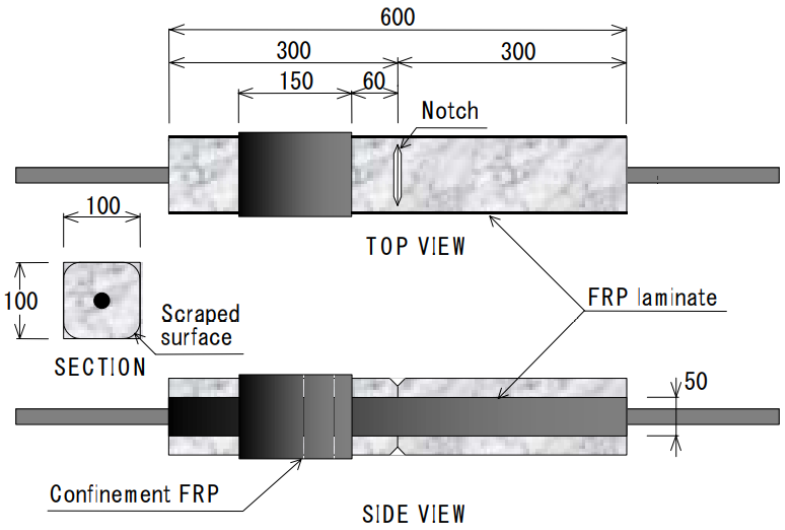

Figure 2-9- Nakaba et al., 2001 test specimen
Source: Nakaba et al., (2001)

Nakaba et al., (2001) found that the maximum load increases as the stiffness of FRP also increases but the maximum local bond stress is not influenced by the type of FRP but increases as concrete compressive strength increases.

A similar study was carried out by Ko & Sato, (2008), where the study variables were the type of FRP and the sheet layers. Cyclic load was applied to the specimens. The test results showed that the maximum load increased, and the ultimate displacement decreased as the elastic modulus, number of layers and thickness of the FRP sheet increased. The inelastic displacements and the stiffness reduction were observed during the repeated unload/reload cycles in the cyclic tests.

Once the problems, the effects, the causes, and the state of the art consulted have been exposed, it is clear the necessity of develop reinforcement methods for RCW to improve their flexural capacities. FRP composites have shown to be a great performance strengthening structural elements, reason why the present research focused on evaluating the behavior of RCW externally reinforced with FRP vertical strips, with the aim of increasing their bending capacities. For this, the behavior of different types of fibers such as CFRP and GFRP was studied, which have been shown to provide different characteristics to the elements reinforced with each one of them.

3. RESEARCH QUESTION AND GOALS

3.1. Research Goals

Assess bending behavior of thin reinforced concrete walls subjected by in-plane lateral load, strengthening with different types of fibers reinforced polymers, FRP.

3.2. Goals

- Evaluate capacity, ductility and failure modes of walls reinforced with different types of FRP bands and different concrete strengths.
- Identify the most favorable type of fiber to retrofit of thin concrete walls with poor vertical reinforcement.
- Analyze and compare the experimental test results and the theorical values calculate by equations of the document ACI 440.2R-17.

4. EXPERIMENTAL PROGRAM

4.1. Overview

The experimental program was designed with the objective of isolating the study variables in the project. The study variables are: influence of different compressive strengths of concrete on the adherence between the sheets and the wall surface, behavior of different reinforcing fibers (CFRP and GFRP) and the incidence of reinforcing the walls with a double layer of sheets.

For this purpose, the anchoring systems was no considered, because the project focused exclusively on the behavior of different types of FRP used as flexural strengthening of RCW and this behavior could be limited by the anchoring system, as observed in the essays of El-Sokkary & Galal in 2013. Additionally, axial load in the walls was not considered either because a flexural failure was sought, and the application of axial load could increase the bending capacities of the walls and induce a shear failure and it could generate failures due to out-of-plane instabilities that were not the objective of the study. It was considered that these two variables should be studied in detail in future research.

The experimental program consisted of six in-plane flexural tests, with cyclical applied load mid-span, performed on reinforced concrete walls with poor flexural internal reinforcement. Four specimens with low concrete strength, 24.1 MPa (3500 psi), and two with high concrete strength, 44.8 MPa (6500 psi), externally bonded fiber-reinforced polymer (FRP) strips were tested. Two different types of fibers, glass fibers (GFRP) and carbon fibers (CFRP) were used for the reinforcement, with the objective of evaluating the influence that different concrete substrate strengths have on the adhesion of the different type of fibers.

This chapter presents the materials characterization, the design of the reinforced concrete walls, construction, and reinforcement with FRP processes, the load protocol and the set-up used for the tests.

4.2. Materials

The physical and mechanical characteristics of the materials used in this investigation are presented below.

4.2.1. Concrete

The structural elements were cast form two types of hydraulic cement concrete, one with high (H) and other with low (L) compressive strengths. The average concrete compressive strengths of each type were determined according to the Norma Técnica Colombiana 673—Colombian Technical Norm, from now on NTC; relatable to ASTM C39—, using concrete cylinders with nominal dimensions of 100 mm x 200 mm (4 in x 8 in). The average concrete compressive strengths for the concretes with low compressive strengths and the one with high compressive strengths, based on three concrete cylinders, were 24.1 MPa (3500 psi) and 44.8 MPa (6500 psi), respectively.

4.2.2. Reinforcing steel

No.4 bars of Steel Grade 420 (Grade 60) were used as longitudinal and transversal reinforcement. The stress-strain curve of the steel was obtained testing one No. 4 bar according to NTC 2289 —relatable to ASTM A706—. As a result of the tests, an average yield strength (fy) of 450 MPa and an average maximum strength (fu) of 621 MPa.

4.2.3. Fiber reinforced polymers (FRP) Fabrics

Three types of Fiber Reinforced Polymers were considered, which consist of two types of Carbon Fiber Reinforced Polymer (CFRP) and one Glass Fiber Reinforced Polymer (GFRP). The two types of CFRP are: High Modulus Carbon Fiber Fabric (CHM), High Strength Carbon Fiber Fabric (CHS). The GFRP is named as High Strength Glass Fiber Fabric (GHS). The same epoxy resin was used with each type of fiber.Fabrics

The properties supplied by the manufacturer are listed below:

- **High Modulus Carbon Fiber Fabric (CHM)**

CHM is a unidirectional carbon fiber fabric, with fiber oriented in the 0° direction. A CHM system is field laminated using two-part 100% solids and high strength structural adhesives. Table 4.1 presents the fiber characteristics.

Table 4.1 - CHM properties

Property	Average Values	Design Values
Tensile Strength	1241 MPa (180 ksi)	1068 MPa (155 ksi)
Modulus of Elasticity	98181 MPa (14.24 x 10^6 psi)	96527 MPa (14.0 x 10^6 psi)
Elongation at Break	1.27 %	1.1%
Thickness	2.03 mm (0.08 in)	
weight	1300 g/m^2 (38 oz/yd^2)	

- **High Strength Carbon Fiber Fabric (CHS)**

Fibers in CHS are oriented in the 0° direction. CHS is field laminated, using two-part 100% solids and high strength structural adhesives to form a CFRP system Table 4.2 presents the fiber characteristics.

Table 4.2 - CHS properties

Property	Average Values	Design Values
Tensile Strength	1240 MPa (180 ksi)	1034 MPa (150 ksi)
Modulus of Elasticity	73770 MPa (10.7 x 10^6 psi)	73770 MPa (10.7 x 10^6 psi)
Elongation at Break	1.7 %	1.4%
Thickness	1.02 mm (0.04 in)	
weight	600 g/m^2 (17.7 oz/yd^2)	

- **High Strength Glass Fiber Fabric (GHS)**

GHS is a unidirectional glass fiber fabric with fiber oriented in the 0° direction with additional yellow glass cross fibers at the 90°. GHS is field laminated using two-part 100% solids and high strength structural adhesives to form a GFRP system. Table 4.3 presents the fiber characteristics.

Table 4.3- GHS properties

Property	Average Values	Design Values
Tensile Strength	567 MPa (82.28 ksi)	487 MPa (70.6 ksi)
Modulus of Elasticity	26680 MPa (3.87 x 10^6 psi)	26680 MPa (3.87 x 10^6 psi)
Elongation at Break	2.13 %	1.8%
Thickness	1.016 mm (0.04 in)	
weight	915 g/m^2 (27 oz/yd^2)	

- **Epoxy Resin**

The epoxy resin is a two-part, 100% solids, epoxy for high strength composite bonding applications. The result of its combination with CFRP and GFRP fabrics provides a wet-layup composite for strengthening of structural members. May be thickened with fumed silica to produce a finishing coat, depending on the project requirements.

4.3. Concrete walls design

The different factors considered for the design of the test specimens were the expected failure mode, the test set-up, how the load would be applied, the hydraulic actuator capacity, and the FRP reinforcement.

4.3.1. Specimen Size

The walls' height represents the height of the walls in typical residential buildings. The chosen dimensions of reinforced concrete walls were a rectangular cross-section, width and thickness, of 1500 x 100 mm (60 x 4 in), with an overall effective height of 2250 mm (88.5 in), resulting in a double total effective height of 4500 mm (177 in). Upper and lower restraints were applied to the specimens at 250 mm (10 in), from each end, therefore, their total height was 5000 mm (197 in), as shown in Figure 4-1.

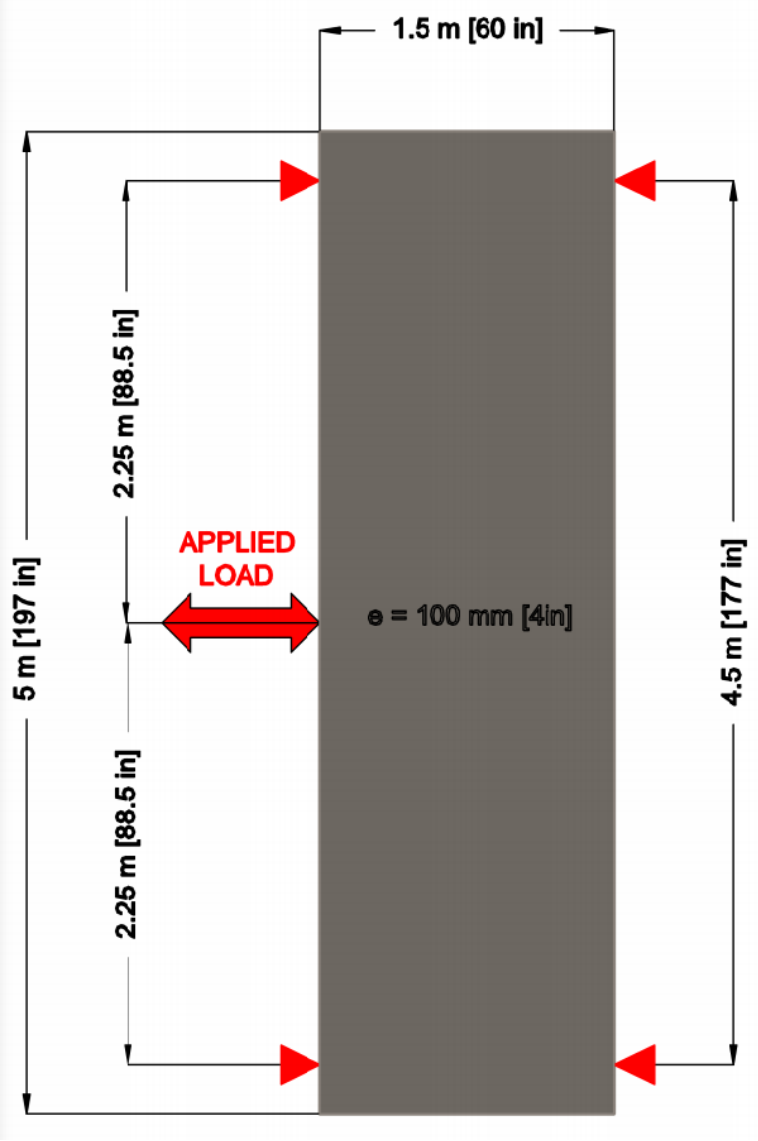

Figure 4-1- Specimen size
Own source

4.3.2. Specimen Layout

The longitudinal reinforcement consisted in seven No. 4 reinforcing steel bars, spaced 230 mm (9 in) from the center. The transverse reinforcement consists of thirty-two No. 4 reinforcing steel bars, set 150 mm (6 in) apart from the center, as shown in Figure 4-2. The average concrete compressive strengths for the concretes with low compressive strengths and the one with high compressive strengths were 24.1 MPa (3500 psi) and 44.8 MPa (6500 psi), respectively.

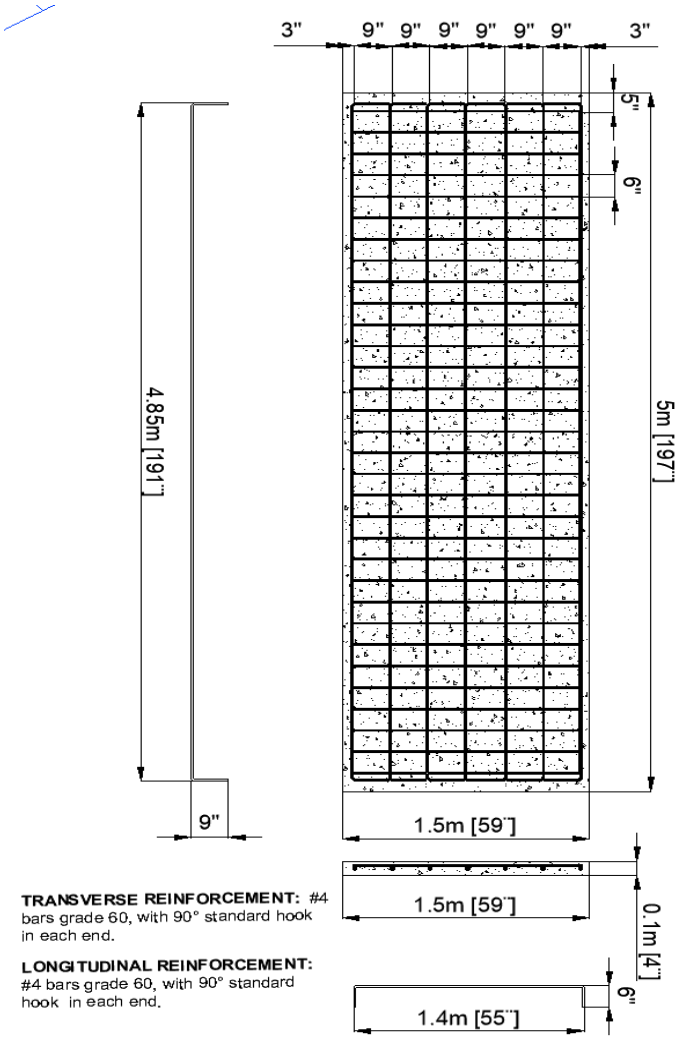

Figure 4-2- Reinforcement layout.
Own source

For both types of specimens (high and low concrete compressive strengths), it was necessary to calculate its ultimate capacity and determine the expected failure mode. This entails the calculation and comparison of the shear and flexion capacities of the walls. These calculations are shown below.

- **Bending capacity**

To calculate the bending capacity of the walls, corresponding interaction diagrams were constructed. The input data needed to build them is shown in Table 4.4.

Table 4.4-Input data for interaction diagram

Property		SI	USCS
Maximun concrete strain	ε_{cu}	0.0030 mm/mm	0.0030 in/in
Yield steel strain	ε_y	0.0021 mm/mm	0.0021 in/in
Modulus of elasticity of steel	E_y	214 GPa	$31x10^3$ ksi
Wall length	l_w	1.50 m	60 in
Wall thickness	t_w	0.10 m	4 in
Effective wall length	d_w	1.424 m	56 in
Concrete strength	f'_c	24.1 MPa & 44.8 MPa	3500 psi & 6500 psi
Steel yield strength	f_y	450 MPa	65.3 ksi

Own source

The interaction diagram for each concrete strength of walls is shown in Figure 4-3.

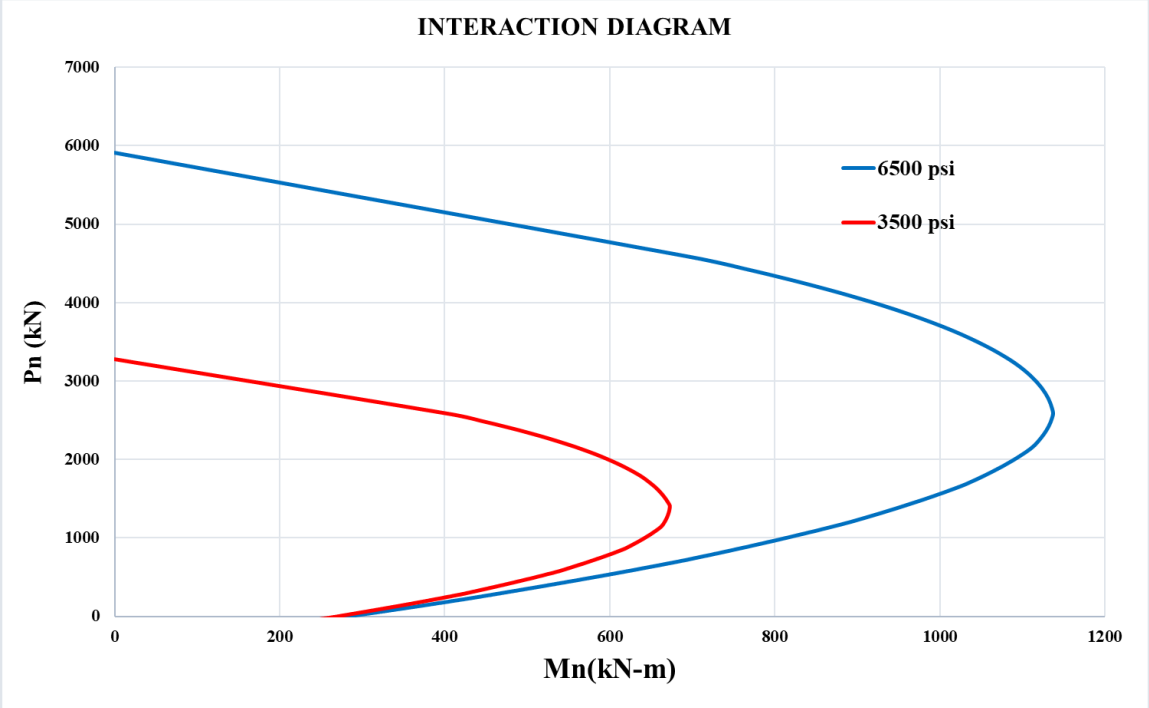

Figure 4-3-Interaction diagram
Own source

No axial loads were intended to be applied to the walls. Therefore, the moment at which there is no axial force is obtained from the interaction diagrams shown in Figure 4-3 for each concrete strength, 272 kN-m (200 kips-ft) for f'c of 3500 psi walls and 281 kN-m (207 kips-ft) for f'c of 6500 psi walls.

- **Shear capacity**

To determine the shear strength of the walls, the following equation was used, which was proposed in the ACI 318-19, under the code 18.10.4.1(ACI 318, 2019).

$$V_n = \left(\alpha_c \cdot \lambda \cdot \sqrt{f'_c} + \rho_t \cdot f_{yt}\right) \cdot t_w \cdot l_w$$

Equation 5

Where:

$\alpha_c = 0.25, for\ \ h_w/l_w \leq 1.5$

$\lambda = 1, \qquad for\ normal\ concrete$

Replacing the values in Equation 5:

$$V_n = \left(0.25 \cdot 1.0 \cdot \sqrt{24.1[MPa]} + 0.00831 \cdot 450\ [MPa]\right) \cdot 100\ [mm] \cdot 1500\ [mm]/1000$$

$V_n = 756\ kN\ (169\ kips)$.

In the same way was determined the shear strength of the 6500 psi compressive strength walls, resulting in a shear resistance of V_n= 823 kN (185 kips).

To determine the failure mode and load it was necessary to compare the ultimate flexural load and the ultimate shear load. For this, the physical model is shown in Figure 4-1, where the wall has simple lateral supports at the top and the bottom, and the load is applied at half wall height.

Table 4.5 shows the ultimate loads for a flexural and shear failure, and the expected failure mode. Tests verified this behavior.

Table 4.5- Comparison between flexural capacity and shear capacity

compressive concrete strength		Ultimate load for flexural failure, P_{nf}		Ultimate load for shear failure, P_{ns}		P_{ns}/P_{nf}	Expected failure mode
MPa	psi	kN	kips	kN	kips		
24,1	3500	242	54	1512	340	6,3	Flexural failure
44,8	6500	250	56	1645	370	6,6	Flexural failure

Own source

4.4. Reinforcement settings

Four specimens were built with low-strength concrete, and two with high-strength concrete. To compare the results, for each of the concrete's compressive strengths there is a control specimen, named L-0 and H-0.

One of the low compressive strength walls was reinforced with high strength fiber glass strips, called L-GHS-1. The other two low strength walls were reinforced with high strength carbon fiber strips, the first with one layer, called L-CHS-1, and the second with two layers, called L-CHS-2. In this way, it was possible to compare the different behaviors provided by the reinforcements with the two types of fibers (GHS and CHS) and, additionally, to review the effects of varying the number of reinforcement layers applied.

The last specimen of high-strength concrete was reinforced with high modulus carbon fibers, named H-CHM-1. Table 4.6 shows the study variables in each of the specimens.

Table 4.6- Study variables

Wall ID	Substrate Strength f´c [psi]	FRP System	Vertical FRP
L-0	3500	-	-
L-GHS-1	3500	High Strength Glass Fiber Fabric	1 ply 8” wide on one face at each end of wall
L-CHS-1	3500	High Strength Carbon Fiber Fabric	1 ply 8” wide on one face at each end of wall
L-CHS-2	3500	High Strength Carbon Fiber Fabric	2 plies 8” wide on one face at each end of wall
H-0	6500	-	-
H-CHM-1	6500	High Modulus Carbon Fiber Fabric	1 ply 8” wide on one face at each end of wall

Own source

4.4.1. Test matrix

All test specimens have been uniquely labeled and identified for quality and traceability using the following format:

N- SSS -X

Where “N” is the associated concrete strength, “SSS” is the specimen’s FRP strengthening, and “X” is the number of FRP strengthening layers. The detailed nomenclature is reported in Table 4.7.

Table 4.7- Specimen identification

Parameter description	Detail	ID
N- Nominal concrete strength	Nominal Low Concrete Strength (3500 psi)	L
	Nominal High Concrete Strength (6500 psi)	H
SSS- Strengthening	Control (unstrengthened)	0
	High Modulus Carbon Fiber Fabric	CHM
	High Strength Carbon Fiber Fabric	CHS
	High Strength Glass Fiber Fabric	GHS
X- Number of FRP´s strengthening layers	One layer	1
	Two layers	2

Own source

The Figure 4-4 shows the schemes reinforcement setting.

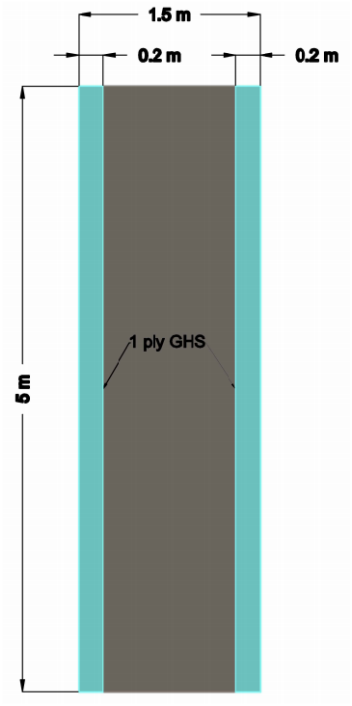

(a) L-GHS-1

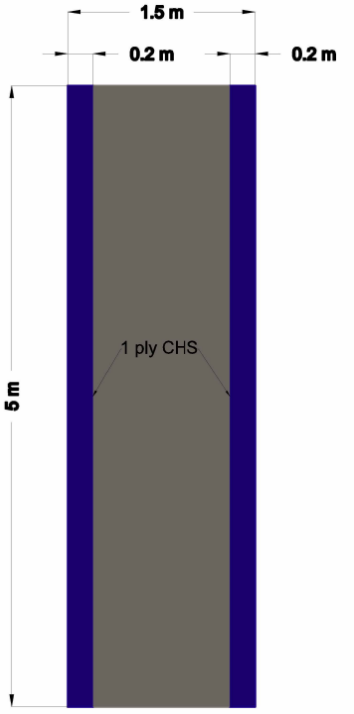

(b) L-CHS-1

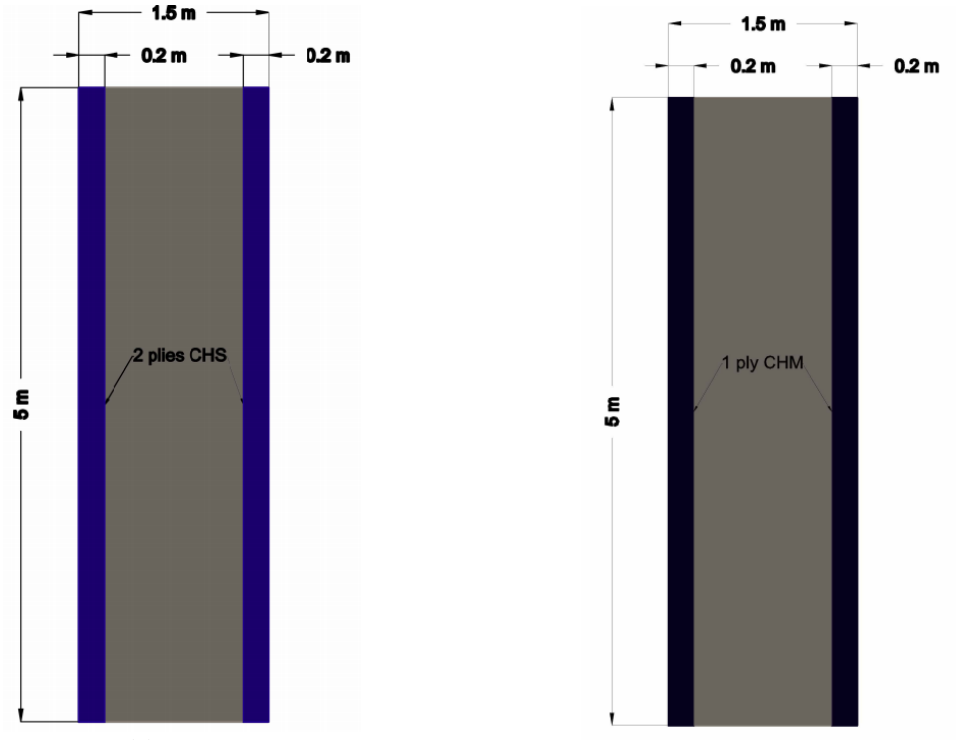

(c) L-CHS-2 **(d) H-CHM-1**

Figure 4-4- Reinforcement settings.
Own source

4.5. Theorical capacity

The theorical capacity of the specimens was calculated based on the ACI 440.2R-17 guidelines.

The limit for the effective strain in FRP will be limited to the strain at which debonding may occur or the strain at which rupture occurs, ε_{fd}, as defined in Equation 1.

Flexural design involves iteration to achieve equilibrium across the section. Annex: FRP reinforcement design contains the design calculation for the FRP contribution for L-GHS-1 specimen and Table 4.8 shows the theorical capacities provided by the FRP reinforcement for each specimen.

Table 4.8- Theorical capacities of specimens.

Specimen ID	$P_{n,cu}$		ΔP_{nFRP}		$P_{n,FRP}$		$P_{n,FRP}/P_{n,cu}$
	kN	kips	kN	kips	kN	kips	
L-0	242	54	--	--	--	--	--
L-GHS-1	242	54	62	14	303	68	1,25
L-CHS-1	242	54	101	23	342	77	1,42
L-CHS-2	242	54	140	32	382	86	1,58
H-0	250	56	--	--	--	--	--
H-CHM-1	250	56	250	56	500	112	2.00

Own source

4.6. Constructive procedure

The specimens were constructed following the walls design exposed in section 4.3. Cylindrical specimens were casted to evaluate the mechanical properties of the concrete. Figure 4-5 shows the construction process.

(e) Reinforcing mesh

(f) Reinforcing mesh centered on the formwork.

(g) Wall casting

(h) Test specimen

Figure 4-5- Constructive procedure.
Own source

4.7. Reinforcement procedure

The preparation and installation of the FRP system was performed following the manufacturer's recommended procedure. This section describes the specimens' reinforcement process, according to the settings explained in section 4.4.

4.7.1. Surface preparation

An adequate bonding of the FRP fibers and the concrete walls is critical to develop the real strengthening system capacity, since the fabrics are going to work like a flexural strengthening. The surface preparations were performed following ICRI No. 310.1R guidelines (ICRI 310.2R, 2013).

To achieve an open-pore texture with a concrete surface profile of CSP-3, according to ICRI No. 310.1R guidelines, a polishing machine was used. This tool helped rough the concrete substrate surface on the areas marked for installation. Subsequently, the surface was cleaned with compressed air to remove any remaining dust and dirt. Figure 4-6 shows the concrete surface after the polishing process.

Figure 4-6- surface preparation after polishing process.
Own source

4.7.2. Preparation of epoxy resin

The epoxy resin consisted of two parts, named parts A and B. First, part A was premixed for two minutes. Later, part B was added to the mix. Finally, both components were blended with a mechanical mixer for three minutes until a smooth, uniform and streak-free consistency was reached. Both components were mixed following the mixing ratio provided by the manufacturer: 100-parts part A to 33 parts part B (by weight).

The thickened epoxy paste used to fill the irregular areas was prepared using the maximum ratio by volume recommended by the manufacturer: 1.5 parts of silica to 1 part of the resin.

4.7.3. FRP application

The reinforcement process consisted of:

1. Marking the designated location of the fiber sheets on the concrete surface.
2. Preparing the concrete surface until achieving a surface roughness of CSP 3 per ICRI (International Concrete Repair Institute).
3. Cutting the fiber sheets to the requirement size.
4. Mixing the epoxy resin and thickened epoxy paste.
5. Filling the irregular's areas with the thickened epoxy paste using a flexible spatula.
6. Placing on a flat surface each pre-cut fiber sheet while pouring and spreading over it the resin, using a flexible spatula.
7. Fully saturating the fiber sheet, using a ribbed roller by rolling in the fiber direction. This process was then repeated on the other side of the fiber sheet to ensure full saturation.
8. Placing the saturated fiber sheet on the specimen's designated location.

9. Ensuring that the installed fiber sheet was aligned, and removing excess resin and air bubbles, using the flexible spatula and ribbed roller.
10. Curing the strengthened specimens in laboratory conditions for a minimum of five days prior to any handling or testing.

Figure 4-7 shows the reinforcement procedure.

(a) Polishing process.

(b) Surface roughness of CSP 3.

(c) Priming of the surface.

(d) Saturating of the FRP fabrics.

(e) FRP application.

(f) FRP applicated.

Figure 4-7- Reinforcement procedure

Own source

4.8. Loading protocol

The theorical ultimate load of the control specimens (L-0 and H-0) was taken as a reference to develop the unreinforced specimens load control protocol. The test speed was set in 900 kg/s.

The load protocol of the unreinforced specimens consisted of three initial steps of 25%, 50% and 75% of the expected load, with only one cycle of each step, followed by a fourth step of 100%, with three cycles and 10% increase until failure. Figure 4-8 shows he load protocol for the control specimens.

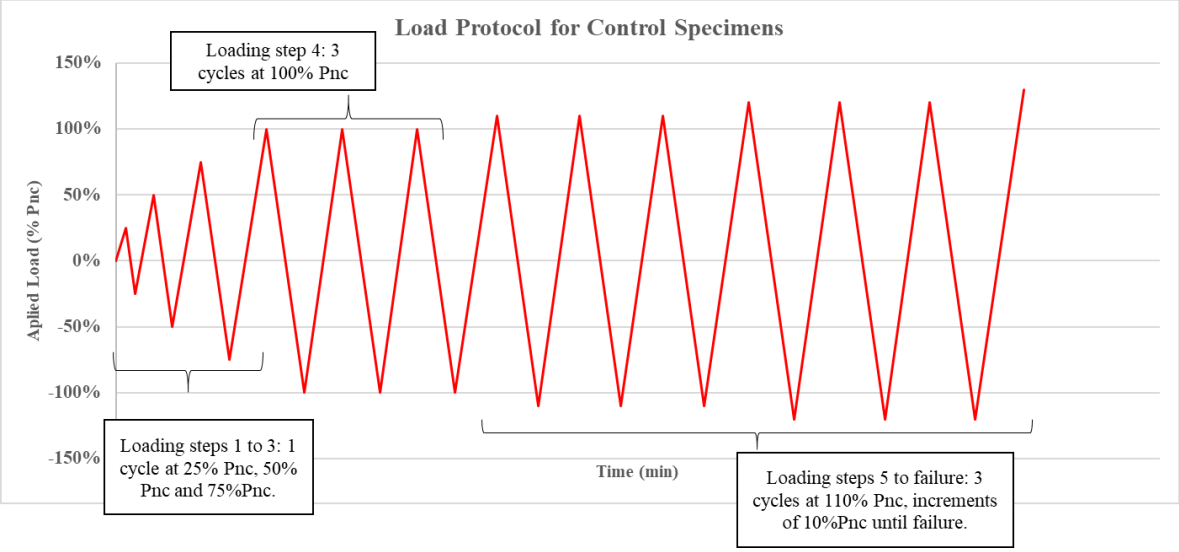

Figure 4-8- Load Protocol for Control specimens.
Own source

For the strengthened specimens, the test was divided in two protocols (a hybrid control). The first protocol was force-controlled and the second was displacements-controlled. The first protocol was based on the theorical capacity for the unreinforced specimens (277 kN for low concrete strength and 234 kN for high concrete strength), performing steps at 25%, 50% and 75% P_{nc}, following a 100% P_{nc} step that consisted in three cycles and five 6% increments. The second protocol was based on the maximum displacement obtained in the last cycle of the force protocol, increasing it in 10% until failure. Figure 4-9 shows he load protocol for the reinforced specimens.

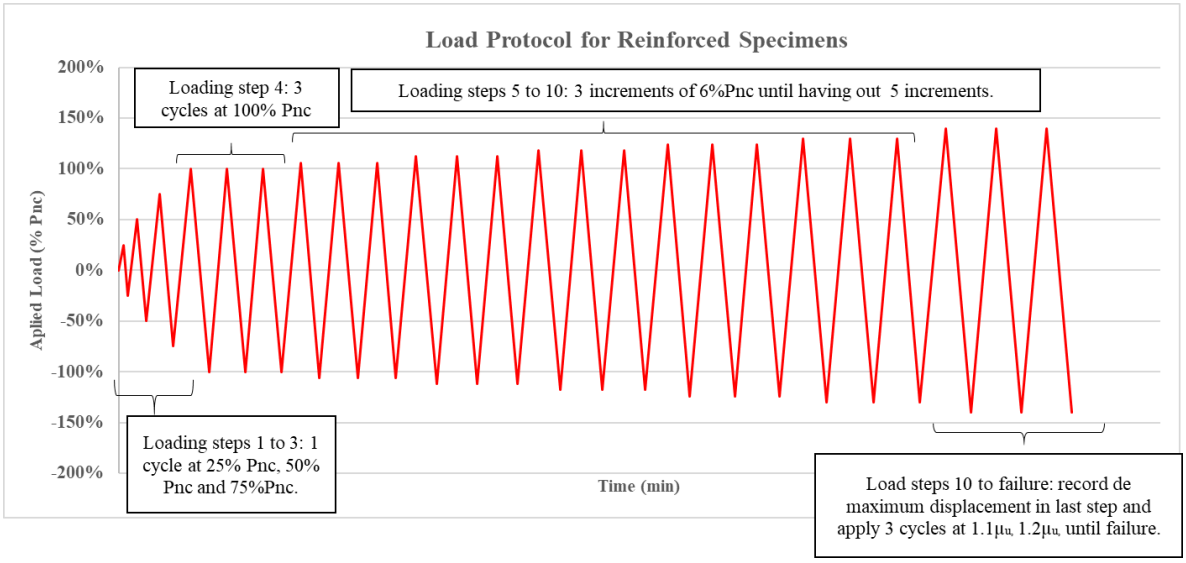

Figure 4-9- Load protocol for reinforced specimens.
Own source

4.9. Test setup and instrumentation

The test setup was designed and validated to ensure controlled test conditions. All specimens were supported along the two shorter sides and secured, via high strength steel threaded bars and plates, to a structural frame to allow for the application of the lateral loads. The load application was made by a MTS hydraulic actuator of 1000 kN (225 kips) of capacity. The lateral displacements were measured with displacement transducers (LVDT's) mounted to a rigid support. The displacement of the frame was also monitored. The test setups are shown in Figure 4-10, and the LVDT's instrumentation is shown in Figure 4-11.

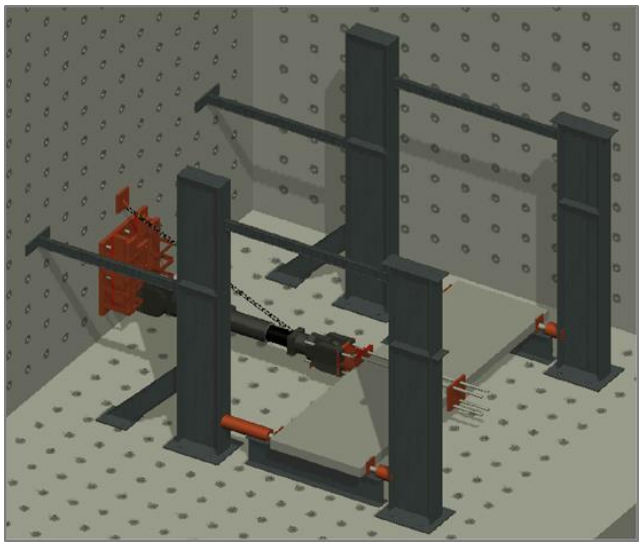

(a) 3D model of the test set- up

(b) Lab view

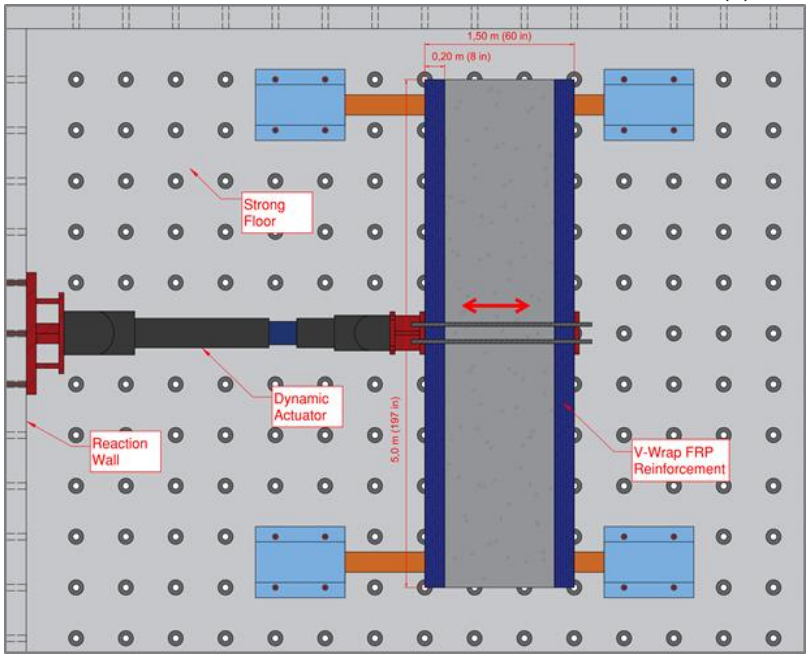

(c) Plant view schematic test set-up

Figure 4-10. Test set-up.

Own source

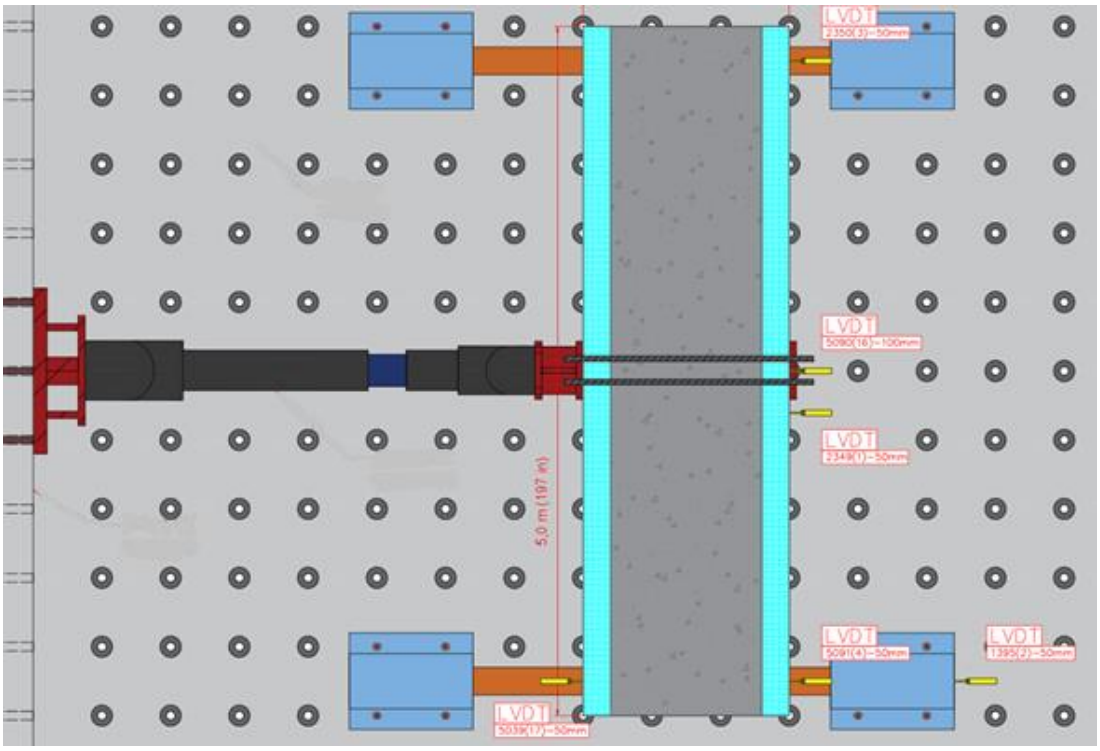

Figure 4-11- Instrumentation of the test
Own source

All specimens were conditioned under laboratory ambient conditions at room temperature 23 ± 1°C (73 ± 3°F) and 50 ± 5% relative humidity, for at least 72 hours prior testing.

5. RESULTS AND ANALYSIS

5.1. Experimental Results Summary

The Table 5.1 show the maximum load results for each wall, with the respective failure mode and the maximum displacements in tension (hydraulic actuator pull) and compression (hydraulic actuator push). The experimental load was compared with the expected theorical load, the experimental/theorical load rate is shown in Table 5.1.

Table 5.1- Results for cyclic (dynamic) in-plane bending wall tests.

Specimen ID	Peak Lateral Experimental Displacement in Tension		Peak Lateral Experimental Displacement in Compression		Peak Lateral Experimental Load in Tension		Peak Lateral Experimental Load in Compression		Peak Theoretical Lateral Load		Exp. Failure /Theo.	Failure Mode
	mm	in.	mm	in.	kN	kips	kN	kips	kN	kips		
L-0	**22.6**	0.89	-14.9	-0.59	**294**	66.1	-294	-66.1	241.5	54.3	1,22	**Flexion**
L-GHS-1	**16.0**	0.63	-13.8	-0.54	**324**	72.8	-360	-80.9	303.0	68.1	1,07	**Debonding**
L-CHS-1	**10.3**	0.41	-10.9	-0.43	**377**	84.8	-405	-91.1	342.0	76.9	1,10	**Debonding**
L-CHS-2	12.0	0.47	**-9.2**	-0.36	481	108.1	**-431**	-96.9	381.8	85.8	1,13	**Debonding**
H-0	**23.6**	0.93	-12.8	-0.50	**301**	67.7	-304	-68.3	249.6	56.1	1,21	**Flexion**
H-CHM-1	**9.7**	0.38	-8.1	-0.32	**421**	94.6	-422	94.9	499.6	112.3	0,84	**Debonding**

The control specimens presented a flexion failure with multiple progressive cracking in the middle of the wall, while the reinforced walls presented the typical failure mechanism of the FRP reinforcement system, where a progressive detachment of the FRP strip until it finally comes off completely.

For low-resistance concrete walls, the control wall (L-0) reached a resistance of 294 kN, which means that it resisted 22% more than the theoretically expected load. The strength of the control wall will be the basis of comparison for all low-strength concrete walls.

The glass fiber reinforced specimen (L-GHS-1) reached an ultimate load of 324 kN, being 7% greater than the theoretically expected load and 10% greater than the control wall (L-0), however the maximum load that the L-GHS-1 specimen resist was 19% greater than the expected theorical maximum load. It is observed that it was the type of fiber that contributed the least resistance to the wall, because it is the fiber with the lowest ultimate stress, however, as it is the fiber with the highest deformation capacity, it is expected that it is the reinforcement that achieves the greatest energy dissipation.

The specimen reinforced with a layer of carbon fibers (L-CHS-1) achieved a failure load 10% higher than expected, while the double-layered specimen (L-CHS-2) presented resistance 13% higher than theoretically expected. However, the specimen with a single layer of reinforcement (L-CHS-1) presented a resistance 28% greater than the resistance presented by the control wall (L-0), while the specimen with a double layer of reinforcement (L-CHS-2) increased it by a 47%. As expected, due to the fact that the double layer reinforcement implies a greater stiffness provided, the specimen with double fiber layer (L-CHS-2) present displacements slightly lower than those presented by the

specimen with a single layer (L-CHS-1), result that agrees with the results obtained by Ko & Sato, (2008), where the resisted load increases and the displacement is reduced as a function of the elastic modulus of the fibers (in this case it is the same for both fibers), the thickness and the number of layers increase.

For high- resistance concrete walls, the control wall (H-0) reached a resistance of 301 kN, 21% more than the theoretically expected load. The strength of the control wall will be the basis of comparison for strengthened high-strength concrete wall (H-CHM-1). The H-CHM-1 specimen reached a resistance 16% lower than the theoretically expected resistance, however it exceeded the resistance of the control specimen (H-0) by 40%.

It is evident that the reinforced walls present greater resistance than the control walls, however the lateral displacements that present these walls, depending on the type of fiber used, are reduced by 29% for the glass fiber, 54% for the reinforced wall with a layer of carbon fiber and 59% for the wall reinforced with a double layer of carbon fiber. These results show that the reinforced walls present less degradation of their rigidity until failure compared to the control walls. Additionally, it is appreciated that the wall reinforced with GFRP (L-GHS-1) allows a greater displacement compared to those reinforced with CFRP (L-CHS-1 and L-CHS-2), therefore the reinforcement system with GFRP presents greater ductility than the CFRP reinforcement system, supporting the results obtained by Sheikh et al., (2002) and Di Luccio et al., (2017).

Figure 5-1 shows the experimentally obtained results against those theoretically expected.

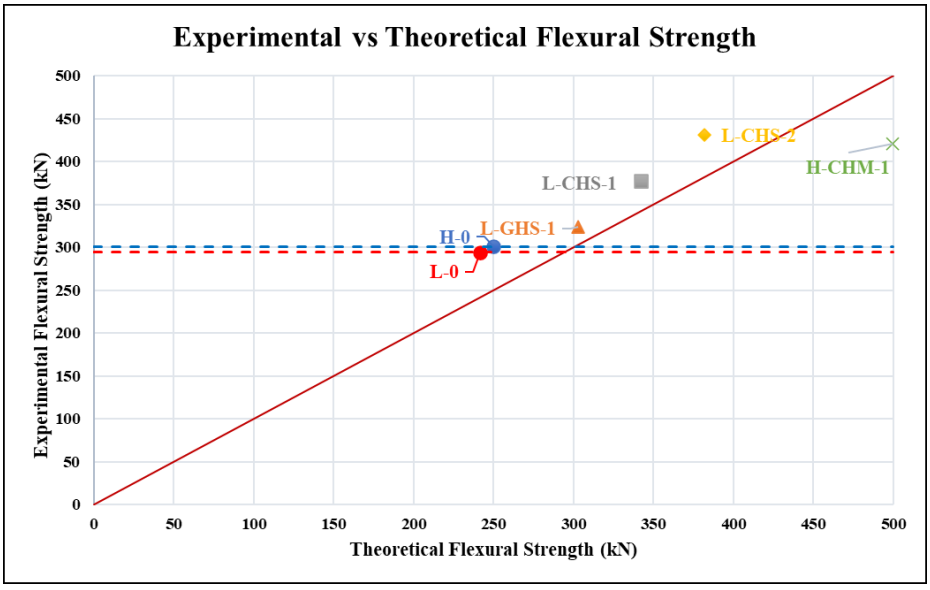

Figure 5-1- Experimental vs theorical capacity.
Own source

All the species reached resistances higher than those theoretically expected, except for the specimen H-CHM-1, which reached a resistance equal to 84% of the expected ultimate resistance. However, it is important to note that the calculated theoretical capacities of the specimens are not reduced by the resistance reduction factor (ϕ).

The Table 5.2 show the gained strength provided by the reinforcement system in each of the specimens.

Table 5.2- Gained strength.

Specimen ID	Maximum Experimental Lateral Load		Gained strength		Strengthened /Control
	kN	kips	kN	kips	
L-0	294	66.1	--	--	1.00
L-GHS-1	324	72.8	30	6.7	1.10
L-CHS-1	377	84.7	83	18.7	1.28
L-CHS-2	431	96.9	137	30.8	1.47
H-0	301	67.7	--	--	1.00
H-CHM-1	421	94.6	120	26.9	1.40

All the strengthened specimens showed a gain in their strength with respect to the control specimen. The wall reinforced with a double layer of carbon fiber (L-CHS-2) has achieved the highest gain of up to 137 kN (30.8 kips), while the fiber with the lowest gain has been the wall reinforced with fiberglass (L-GHS-1) with 30 kN (6.7 kips). It was evidenced that the wall with high compressive strength concrete reinforced with carbon fibers (H-CHM-1) presents a greater resistance gain than the wall with high compressive strength concrete reinforced with carbon fibers (L-CHS-1), a result that is consistent with the obtained by Ko & Sato, 2008.

5.2. Failure mode

This chapter provides a qualitative description of the failure modes obtained in each of the test walls subjected to the cyclic test.

5.2.1. Expected failure mode

To predict the expected failure mode, a comparison has been made between the theoretical shear failure load values (P_{ns}) and the flexural failure load (P_{nf}) for each specimen. As a result, all specimens are expected to exhibit flexural failure.

Table 5.3- Expected failure mode.

Specimen ID	Utimate load for a flexural failure, Pnf		Ultimate load for a shear failure, Pns		Pns/Pnf
	kN	kips	kN	kips	
L-0	242	54	1512	340	6.3
L-GHS-1	303	68	1512	340	5.0
L-CHS-1	342	77	1512	340	4.4
L-CHS-2	382	86	1512	340	4.0
H-0	250	56	1645	370	6.6
H-CHM-1	500	112	1645	370	3.3

The specimens without FRP reinforcement are expected to present multiple cracks in the central third of the wall, generating a progressive plasticization of the section. While the specimens reinforced with FRP, the failure was expected to occur due to debonding of the FRP bands to the concrete surface, because the limit strain calculated by means of Equation 1 gives as a result that the debonding deformation (ε_{fd}) is less than the ultimate strain (ε_{fu}) of the fibers.

5.2.2. L-0 Specimen

Figure 5-2 shows the failure mode for L-0 specimen. The failure mode was flexural failure, with multiple flexural cracking in the middle third, as expected. The failure occurred in the first tension cycle (the hydraulic actuator was pulling) at 120% P_{nc}.

Figure 5-2 Failure mode L-0 Specimen.
Own source

5.2.3. L-GHS-1 Specimen

Figure 5-3 shows the failure mode for L-GHS-1 specimen. The test specimen presented a multiple flexural cracking and pumping of the fabrics in the middle third, followed by FRP debonding. The first fabric was totally detached from the concrete surface, and the second fabric presented pumping in the crack zone but never detached full. The specimen exceeded the load control and reached a load at 1.5 μ_u up to failure, when the actuator was pulling in the tension cycle.

Figure 5-3 Failure mode L-GHS-1 Specimen.

Own source

A debonding failure mode was presented by the specimen, in Figure 5-3 it is observed that the fiber detached from the concrete surface, pulling off small pieces of concrete, however without detaching a uniform layer.

5.2.4. L-CHS-1 Specimen

Figure 5-4 shows the failure mode for L-CHS-1 specimen. The test specimen presented a multiple flexural cracking and pumping of the fabrics in the middle third, followed by FRP debonding. The second fabric was totally detached from the concrete surface, and the first fabric presented pumping in the crack zone but never detached full. The specimen exceeded the load control and reached a load at 1.3 μ_u up to failure, when the actuator was pushing in the compression cycle.

Figure 5-4 Failure mode L-CHS-1 Specimen.

Own source

A debonding failure mode was presented by the specimen, in Figure 5-4 it is observed that the fiber detached from the concrete surface, pulling off a thin and uniform layer of the concrete surface.

5.2.5. L-CHS-2 Specimen

Figure 5-5 shows the failure mode for L-CHS-2 specimen. The test specimen presented a multiple flexural cracking and pumping of the fabrics in the middle third, followed by FRP debonding. The first fabric was totally detached from the concrete surface, and the second fabric presented pumping in the crack zone but never detached full. The first crack came out at 75% P_{nc} in the tension cycle, the same than the failure. The specimen exceeded the load control and reached a load at 1.5 μ_u up to failure, when the actuator was pulling in the tension cycle.

Figure 5-5 Failure mode L-CHS-2 Specimen.
Own source

A debonding failure mode was presented by the specimen, in Figure 5-5 it is observed that the fiber detached from the concrete surface, pulling off small pieces of concrete, however without detaching a uniform layer.

5.2.6. H-0 Specimen

Figure 5-6 shows the failure mode for H-0 specimen. The failure mode was flexural failure, with multiple flexural cracking in the middle third, as expected. The failure occurred in the first compression cycle (the hydraulic actuator was pushing) at 130% P_{nc}.

Figure 5-6 Failure mode H-0 Specimen
Own source

5.2.7. H-CHM-1 Specimen

Figure 5-7 shows the failure mode for H-CHM-1 specimen. The test specimen presented a multiple flexural cracking and pumping of the fabrics in the middle third, followed by FRP debonding. The first fabric was totally detached from the concrete surface, and the second fabric presented pumping for the most of its length but never detached full. The specimen exceeded the load control and reached a load at 130% P_{nc} up to failure, when the actuator was pulling in the tension cycle.

Figure 5-7 Failure mode H-CHM-1 Specimen

Own source

A debonding failure mode was presented by the specimen.

All the specimens presented a flexural failure as expected, the specimens reinforced with FRP presented a sudden failure due to the debonding of the sheets from the concrete surface. The debonding process in the four cases was similar, where the fiber began to detach in the center of the light where the stresses were maximum and the cracking of the concrete had greater presence, cycle by cycle the fibers were detaching more and more until they were detached by full.

5.3. Hysteretic Response

To compare the performance of test specimens, it is helpful to plot the envelopes of the hysteretic cycles of the specimens with the same concrete strength on a single graph. In this way it will be possible to evaluate and compare ultimate capacities, deformation capacity, degradation of stiffness and ductility of the specimens. Figure 5-8 and Figure 5-9 show the hysteretic cycles envelopes for the low concrete strength specimens and high concrete strength specimens, respectively.

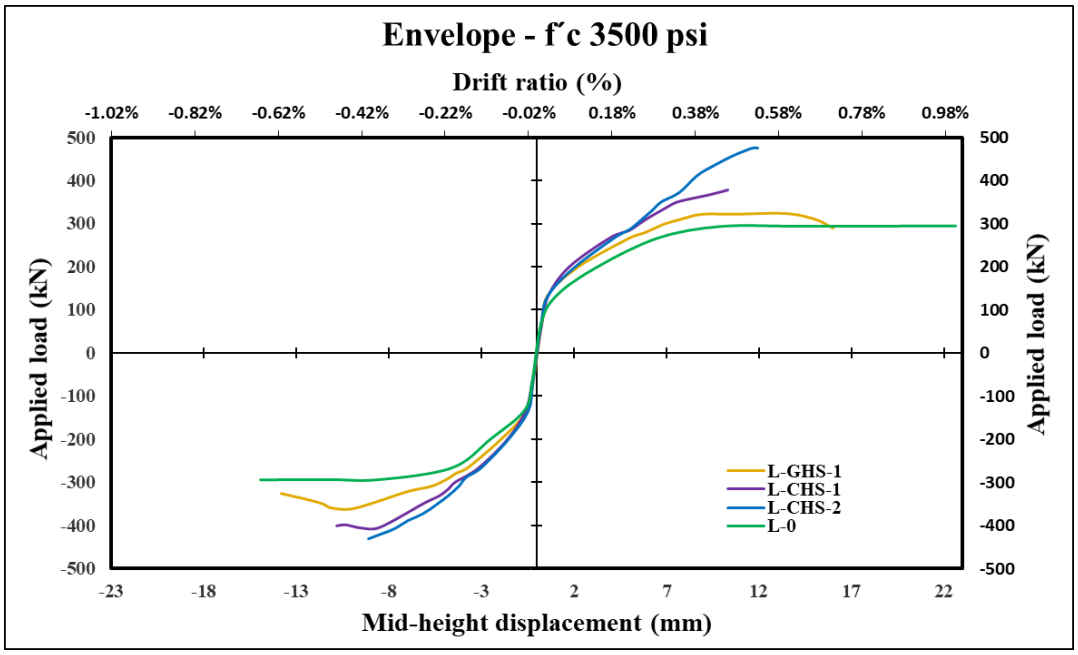

Figure 5-8-Envelope for f´c 3500 psi specimens.

Own source.

The reinforced specimens show a linear and elastic behavior up to displacements of the order of 0.6 mm (0.024 in), while the control specimens show greater displacements in the elastic range of the order of 1 mm (0.039 in). From these values, the walls enter the inelastic range due to the transverse cracking that occurs in the walls, which with loading and unloading cycles produces an increase and prolongation of cracks. These cracks produce a stiffness degradation of the walls, which is evidenced in the decrease in the load-bearing capacity of the walls. The fiberglass reinforced wall (L-GHS-1) reaches the yield of the section before presenting failure due to the fiber debonding, with more displacement but lower ultimate load than other fibers.

Specimens externally reinforced with FRP show a reduction in their ductility. The fibers with the least reduction in ductility were glass fibers, which, thanks to their low modulus of elasticity and high deformation capacity, allow greater deformations in the concrete, greater cracking, and therefore inelastic behavior. This behavior agrees with the results obtained by Sheikh et al., (2002).

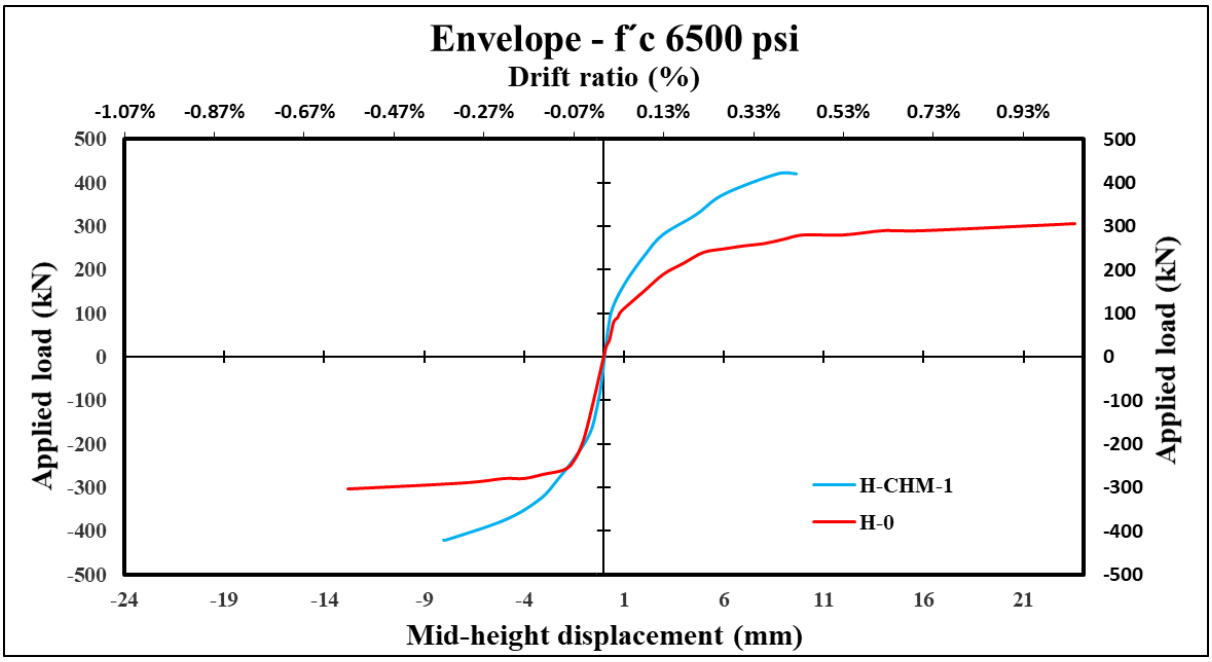

Figure 5-9-Envelope for f´c 6500 psi specimens.
Own source.

The control walls (L-0 and H-0) present a ductile behavior, with a significant incursion into the inelastic range until reaching a completely ductile failure. The walls reinforced with carbon fibers (L-CHS-1, L-CHS-2, and H-CHM-1) practically do not present a yield of the section, this because the reinforcing fibers prevent cracking, when the cracks begin to increase significantly due to the increase in applied load, the fiber exceeds their effective deformation and their debonding failure occurs.

The Figure 5-10 shows the envelopes of the control specimens, where it is evidenced that both specimens presented a very similar ductile behavior. The use of different concrete strengths did not present a significant variation in the behavior of the control walls, in this way, it is possible to compare the behavior of the adhesion between the fibers to different strengths of the concrete substrate.

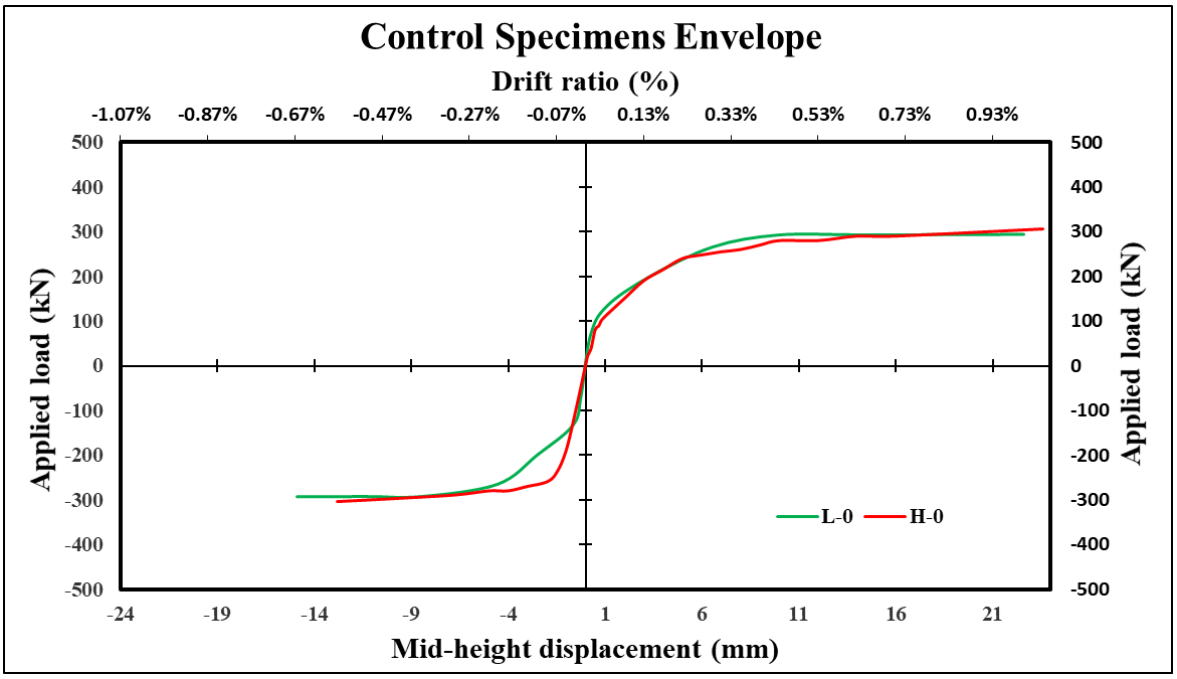

Figure 5-10-Control specimens' envelope.

Own source.

The Figure 5-11 shows the envelopes of the specimens reinforced with FRP, it is evident that the wall reinforced with glass fibers (L-GHS-1) is the wall that presents the most ductile behavior, while the walls reinforced with carbon fibers present the most fragile behavior. On the other hand, comparing the L-CHS-1 and H-CHM-1 walls (both reinforced with carbon fibers with equal tensile strength but different elastic modulus), the wall with high compressive strength concrete (H-CHM-1) presents higher ultimate resistance, reaching an ultimate resistance 17% greater than that of the wall with low-resistance concrete (L-CHS-1). These results agree with the results obtained by Nakaba et al., (2001), where the bond stress is not influenced by the type of FRP but increases as concrete compressive strength increases. Therefore, increasing the strength of the concrete substrate improves the adhesion between the FRP sheets and the concrete and allows the FRP to better develop its expected strength.

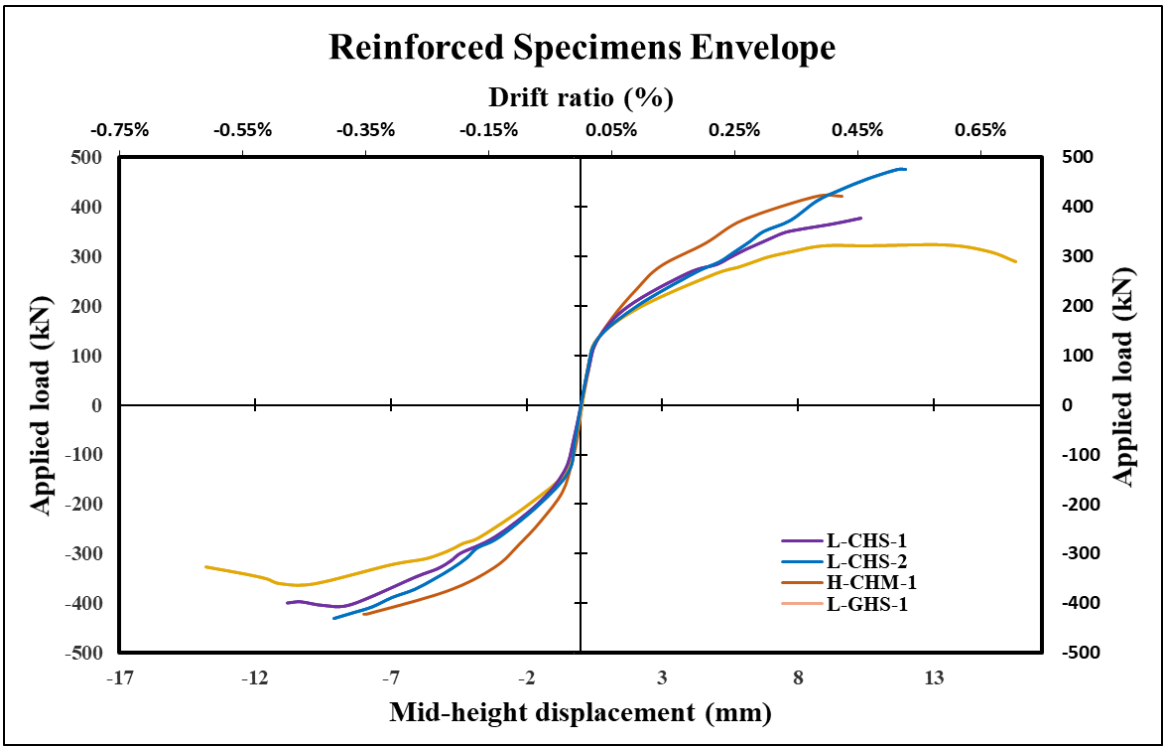

Figure 5-11-Reinforced specimens' envelope.

Own source.

5.4. Stiffness Degradation

The stiffness of the test walls corresponds to slope of each loop that make up the hysteresis cycles presented in Annex A. This slope was calculated as the relationship between applied load and mid-high displacement in each loop. Figure 5-12 and Figure 5-13 show the stiffness degradation of low strength concrete specimens and high strength concrete specimens respectively in each cycle.

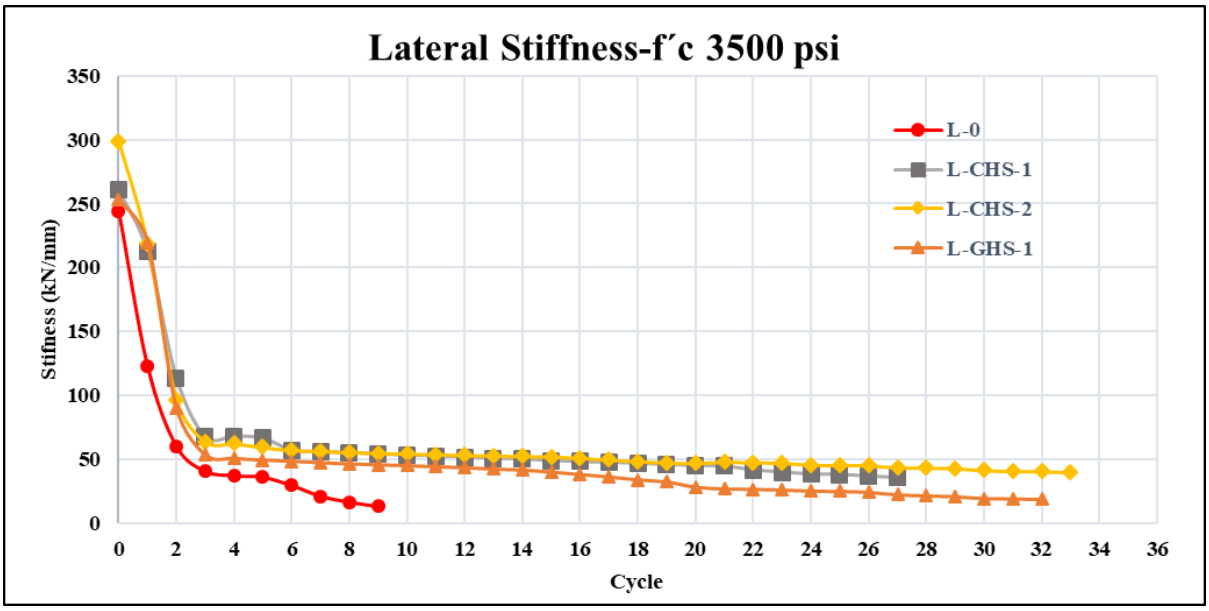

Figure 5-12- Stiffness degradation, low strength specimens (f´c 3500 psi)
Own source.

The initial stiffness of the unreinforced low-strength concrete wall (L-0) was 244.4 kN/mm and presented a reduction of 95% of its initial stiffness, until reaching a final stiffness before failure of 13.0 kN/mm. As expected, the stiffness of the unreinforced wall is the least of the low-strength concrete walls, followed by the glass-fiber-reinforced wall (L-GHS-1), which presented an initial stiffness of 253.2 N/mm, a 4% higher than the initial stiffness of the control wall (L-0), reducing its stiffness up to 93% of the initial one.

Both specimens of low-strength concrete reinforced with carbon fibers (L-CHS-1 and L-CHS-2) showed a reduction of their stiffness of 86% with respect to their initial stiffnesses. The difference is that the double-layer reinforced wall (L-CHS-2) presented an initial stiffness 22% greater than the initial stiffness of the control wall (L-0), while the single-layer reinforced wall (L-CHS-1) increased only one 7% the initial stiffness of the wall.

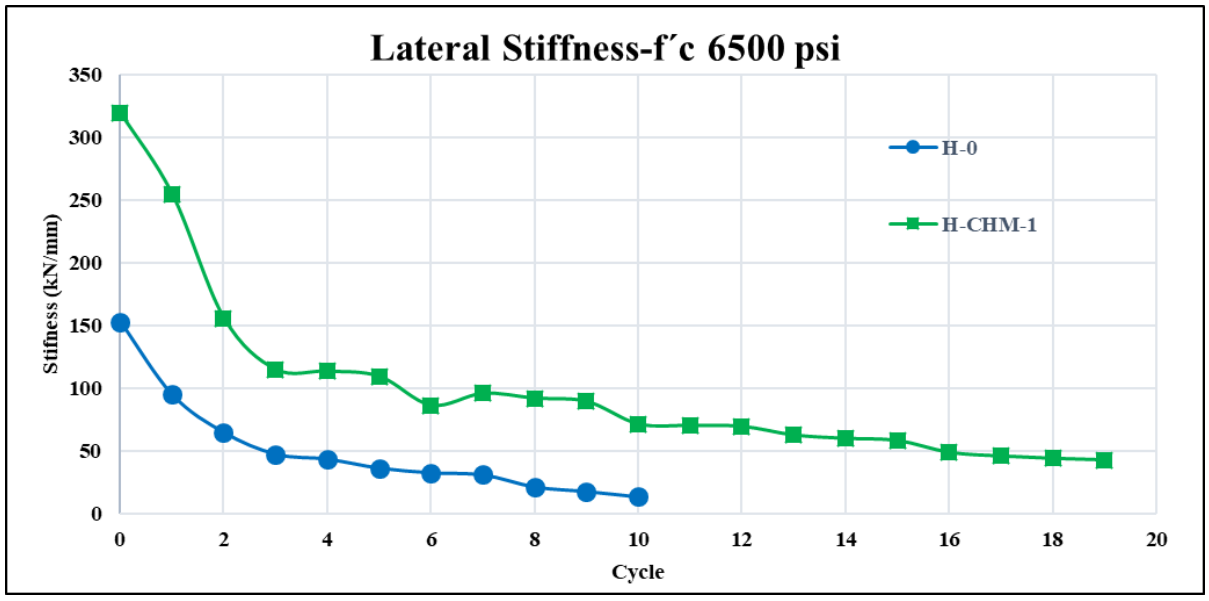

Figure 5-13- Stiffness degradation, high strength specimens (6500 psi).
Own source.

The unreinforced specimen of high-strength concrete (H-0) presented an initial stiffness of 152.9 kN/mm and a reduction of its stiffness before failure of 91%. The specimen reinforced with high modulus of elasticity carbon fiber (H-CHM-1) presented a stiffness of twice the initial stiffness of the control wall (H-0) and presented a reduction of its initial stiffness of almost 87%, up to a stiffness of 42.6 kN/mm.

All the specimens show a sudden reduction in stiffness until reaching the third cycle, however, from here on, the externally reinforced walls show a reduction in the speed with which their lateral stiffness degrades, compared to the control walls that continue to lose stiffness at a rapid rate.

The fiber reinforcement system proved to be an efficient system to increase the initial stiffness of concrete walls, in the same way that was observed in the tests carried out by C. A. Cruz-Noguez et al., (2015). Carbon fibers showed a greater contribution to the initial stiffness of the wall, due to their higher elastic modulus compared to glass fibers. It is observed that the lateral stiffness of the reinforced walls increases as the stiffness of the fiber's increases.

5.5. Ductility

Because the walls do not meet the seismic specifications of the design standards, the calculated energy dissipation coefficients cannot be considered representative of FRP reinforced walls, however, it is of great importance to compare the ductility between reinforced walls with FRP with respect to the control walls. The Paulay and Priestley´s methodology to determinate the ductility and energy dissipation capacity were used to calculate the basic energy dissipation coefficient (R_0) for the test specimens and to be able to determine if the FRP strengthening increases or reduces the energy dissipation capacity.

These methodologies are based on the principles of energy equalization and displacement equalization. Where, in structures with long natural periods its observed that maximum displacement achieved by the inelastic system are very similar to those obtained from an elastic system with the same stiffness as the inelastic system, with unlimited strength, as shown Figure 5-14 (a), where the ductility of the inelastic system is approximately equal to the force reduction factor ($\mu=R_0$).

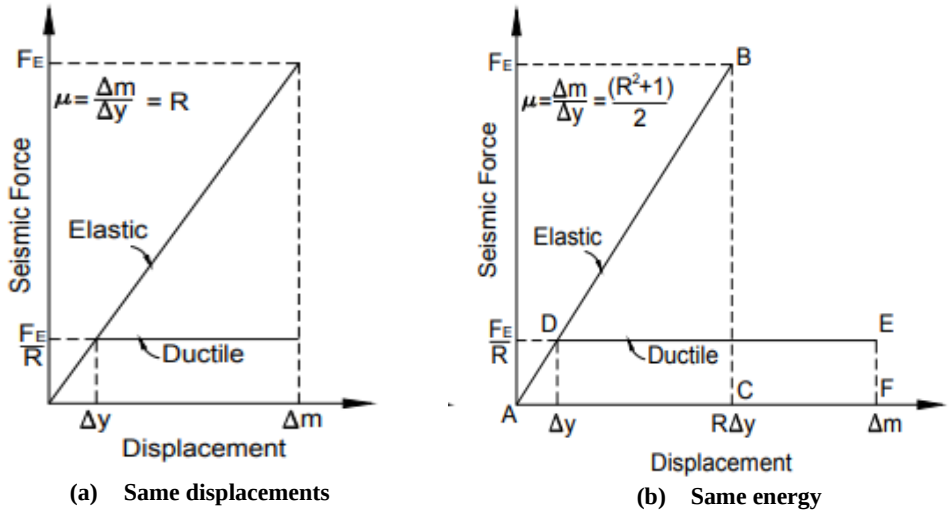

Figure 5-14- Relationship between ductility and force reduction factor.
Source: (Paulay & Priestley, 1992)

For shorter-period structures, this assertion is not very conservative, and it is more appropriate to estimate the value of R by equating elastic and inelastic energies. equating the areas of the triangle ABC and the trapezoid ADEF shown in Figure 5-14, the result is $\mu=(R^2+1)/2$ (Paulay & Priestley, 1992). The authors propose the next expressions to calculate the reduction force factor:

$$\text{Long periods} \rightarrow R = \mu$$

$$\text{Short periods} \rightarrow R = \sqrt{2\mu - 1}$$

$$T=1 \rightarrow R = 1$$

Equation 6
Source: (Paulay & Priestley, 1992)

Where μ is the ductility, where by definition represents the relationship between the maximum strain Δ_m and the yield strain Δ_y.

$$\mu = \frac{\Delta_m}{\Delta_y}$$

Equation 7
Source: (Paulay & Priestley, 1992)

The maximum strain (Δ_m) and the yield strain (Δ_y) were obtained from the envelopes of the hysteresis curves shown in the Figure 5-8 and Figure 5-9, that is shown individually in the Figure 5-15, to calculate the basic energy dissipation capacity factor R_0.

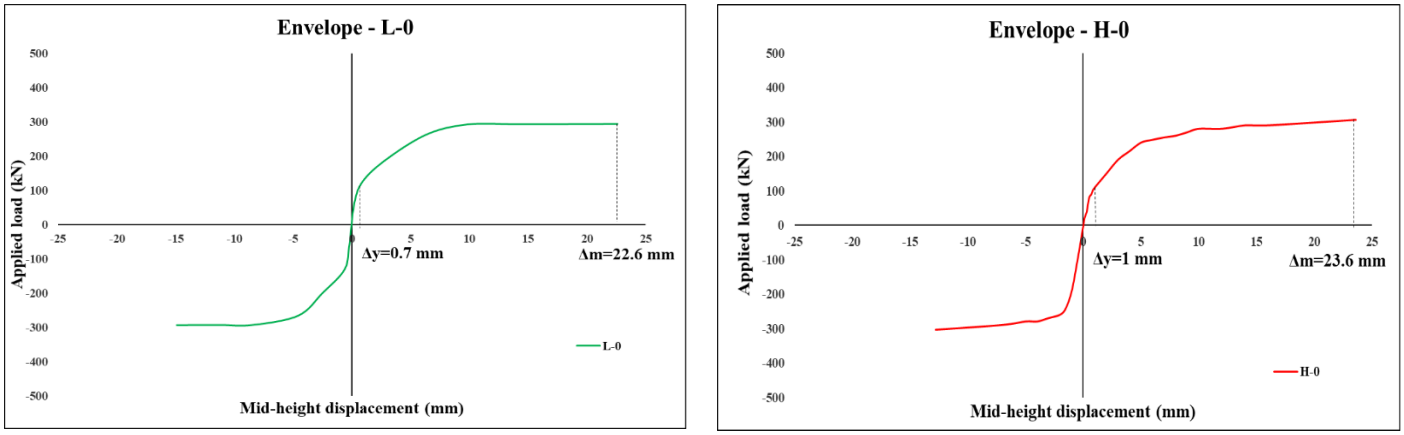

Figure 5-15- Δy and Δm values definition for control specimens (unreinforced).
Own source.

The Table 5.4 shows a summary of the values of the maximum strain (Δ_m) and the yield strain (Δ_y), with the ductility (μ) calculated and the corresponding basic energy dissipation factor defined for short periods (R_0) for the control walls.

Table 5.4-Control specimens R_0 values.

Specimen ID	Δy mm	Δm mm	μ	R_0
L-0	0.7	22.6	32.3	8.0
H-0	1	23.6	23.6	6.8

Considering that these are walls that were designed with a detail that does not meet the seismic requirements of the NSR-10. The walls have poor flexural reinforcement and abundant shear reinforcement, thus ensuring a ductile behavior of the section. This is why the values of the basic coefficient of energy dissipation obtained from the control specimens are higher than those suggested in title A of the NSR-10 for concrete walls with special energy dissipation capacity (DES), which is R_0=5 (NSR-10, 2012).

Figure 5-16 shows the maximum strain (Δ_m) and the yield strain (Δ_y) definition for reinforced specimens.

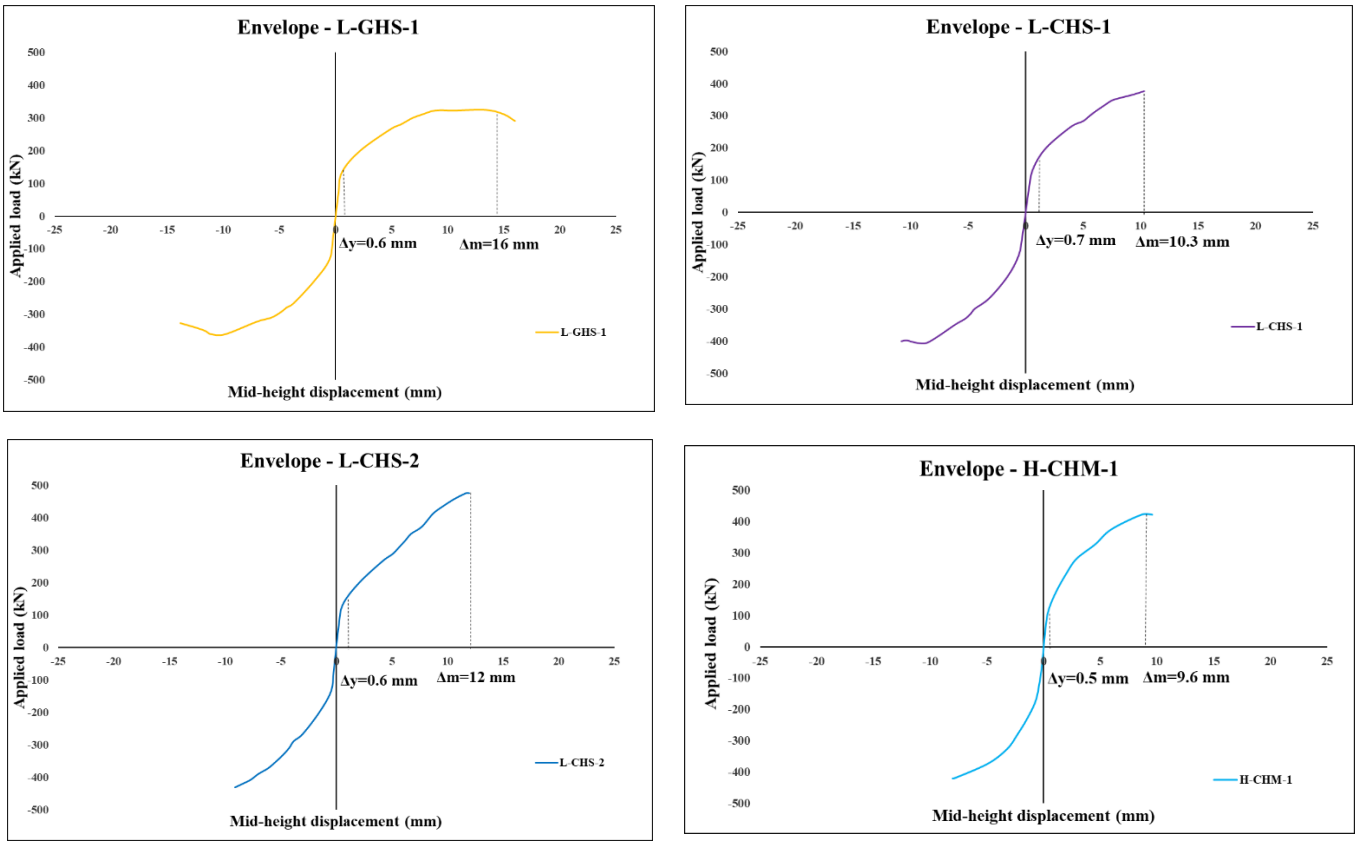

Figure 5-16- Δy and Δm values definition for reinforced specimens.
Own source.

The Table 5.5 shows a summary of the values of the maximum strain (Δ_m) and the yield strain (Δ_y), with the ductility (μ) calculated and the corresponding basic energy dissipation factor defined for short periods (R_0) for the strengthened walls and the comparison between control walls and strengthened walls.

Table 5.5- R_0 values comparison between control specimens and strengthened specimens.

Specimen ID	Δy mm	Δm mm	μ	R_0	R_0 /R_0 control walls
L-GHS-1	0.6	16	26.7	7.2	0.91
L-CHS-1	0.7	10.3	14.7	5.3	0.67
L-CHS-2	0.6	12	20.0	6.2	0.78
H-CHM-1	0.5	9.6	19.2	6.1	0.77

The Table 5.5 results shows that the glass fiber strengthening presented ductility compared to carbon fibers strengthening, however it presents a reduction of the ductility of 9% compared to the control wall (L-0).

The carbon fiber strengthened specimens showed an important decrease in energy dissipation capacity. This behavior can be explained since the glass fibers have a lower elastic modulus (E) and a greater elongation capacity than the carbon fibers.

5.6. Energy dissipation capacity

The failure mode of the elements depends, among other factors, on the energy dissipation capacity, which is a structural property of reinforced concrete elements. Structures subject to seismic events are capable of dissipating energy through hysterical behavior. The energy dissipated by an element subjected to cyclic loads can be quantified as the area under the hysteresis loops and the energy dissipation capacity is calculated as the accumulation of the energy dissipated in all the hysteretic loops (Shen et al., 2017). The Figure 5-17 shows the energy dissipated by a hysteretic loop.

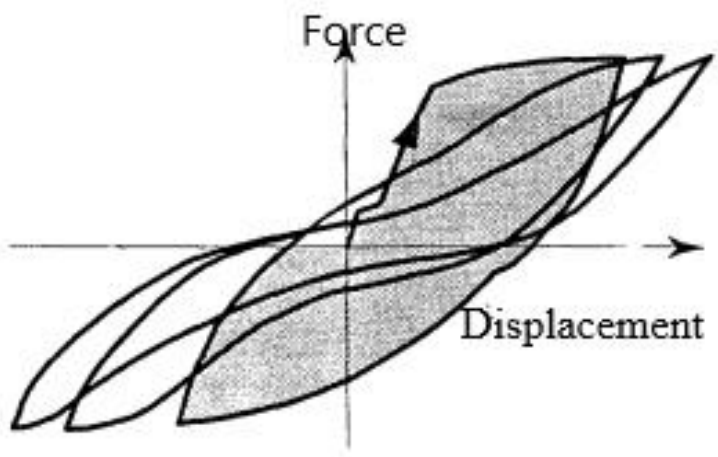

Figure 5-17- Energy dissipated by a cycle
Source: (García R., 1998)

The Figure 5-18 shows the accumulated energy dissipation of the low strength concrete specimens. The unreinforced specimen of low concrete strength (L-0) dissipates 20.1 kN-m. The glass fiber reinforced specimen (L-GHS-1) is the specimen that dissipates the greatest amount of energy among all the specimens, about 220 % more than the control wall (L-0), this important energy dissipation capacity is due to its low elastic modulus and high deformation capacity of glass fibers compared to carbon fibers. The specimen reinforced with a single layer of carbon fiber (L-CHS-1) has a low energy dissipation capacity, even a lower capacity than the control specimen (L-0), reaching a dissipation capacity of the 79% of the control wall capacity.

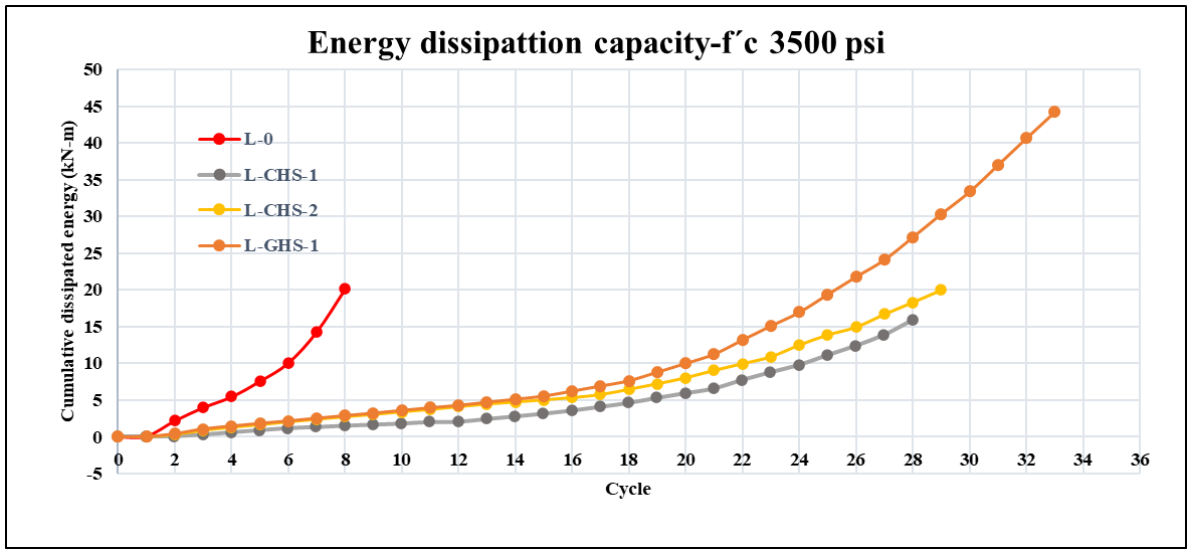

Figure 5-18- Energy dissipation capacity (f´c 3500 psi).
Own source.

The Figure 5-19 shows the accumulated energy dissipation of the high strength concrete specimens. The unreinforced specimen of high concrete strength (H-0) dissipates 16.7 kN-m. The H-CHM-1 specimen dissipated 14.9 kN-m, 11% less than the control specimen.

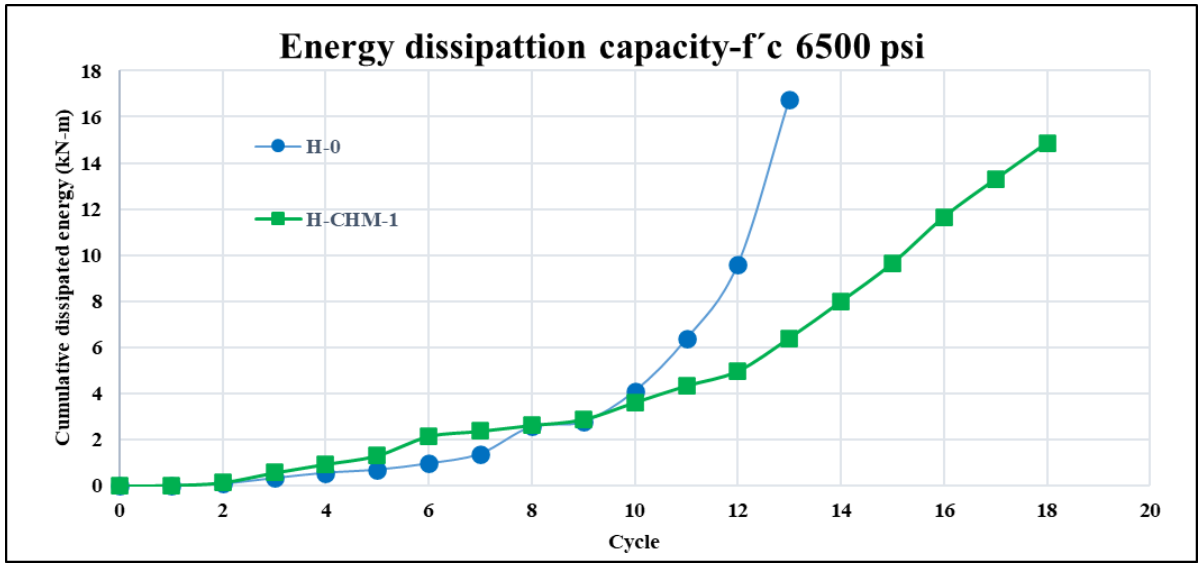

Figure 5-19- Energy dissipation capacity (f´c 6500 psi).
Own source.

The Table 5.6 shows the total energy dissipation of each of the specimens and a comparison between each specimen with respect to its respective control wall. It is evident that fiberglass is the one that

provides the highest energy dissipation capacity to the wall, due to its significant deformation capacity compared to other types of fibers.

Table 5.6- total energy dissipated by each specimen

Specimen ID	Total energy dissipated kN-m	Specimen/ Control
L-0	20.1	-
L-GHS-1	44.2	2.20
L-CHS-1	15.9	0.79
L-CHS-2	20.0	0.99
H-0	16.7	-
H-CHM-1	14.9	0.89

5.7. Results Comparison

Below is a comparison between the results obtained experimentally in the trials and those calculated by design following the methodology proposed in ACI 440.2R-2017 document. Table 5.7 shows the values of maximum lateral load resisted by the test specimens in the tests and the theoretically calculated, without reducing the values by the resistance reduction factor (ϕ); the calculation of the factor of security that corresponds to the relationship between the values obtained experimentally and the theoretical calculated loads.

Verifying the safety factors obtained, it is found that, in general, the procedures established in the design guide are on the side of the structural safety, however the H-CHS-1 specimen presents resistance lower than expected.

Table 5.7- Comparison of experimental and theoretical results.

Specimen ID	Lateral Experimental Load		Theoretical Lateral Load		Security Factor
	kN	kips	kN	kips	
L-0	294	66	242	54	1.22
L-GHS-1	360	73	303	68	1.07
L-CHS-1	405	85	342	77	1.10
L-CHS-2	431	97	382	86	1.13
H-0	304	68	250	56	1.21
H-CHM-1	422	95	500	112	0.84

6. CONCLUSIONS AND RECOMMENDATIONS

6.1. Conclusions

Based on the results obtained in the research project, the following conclusions are presented:

- The vertical FRP sheets externally bonded at the ends and on one face of the wall with the purpose of enhancement the flexural capacity of a reinforced concrete wall showed great performance, increasing the capacity.
- The predominant failure mode for the flexural FRP reinforcement of the wall is debonding, due to the large deformations to which the fibers located on the ends of the wall are subjected.
- The walls reinforced with CFRP showed greater increase in the ultimate capacities (a single FRP layer specimens), compared to the wall reinforced with GFRP (L-GHS-1).
- The external reinforcement with vertical FRP bands located at the ends of the wall, on one of its sides, increases the initial lateral stiffness and delayed stiffness degradation.
- The specimen that presented the highest energy dissipation capacity was the GFRP-reinforced specimen (L-GHS-1). While all CFRP-reinforced specimens show a reduction in energy dissipation capacity compared to control walls.
- Specimens externally reinforced with FRP show a reduction in their ductility. The fibers with the least reduction in ductility were glass fibers (GFRP), due to their low modulus of elasticity and high deformation capacity.
- Carbon fibers (CFRP) have proven to be the most favorable type of fiber to retrofit of thin concrete walls with poor vertical reinforcement, because it has shown greater benefits by increasing the ultimate capacities for bending and lateral stiffness of the walls.
- The capacities of the walls calculated following the procedure proposed in the document ACI-440.2R shows a correct correlation with the results obtained experimentally for the concrete specimens. Therefore, it can be concluded that the methodology proposed in the document, based on the classical flexural theory of concrete combined to strains compatibility, is adequate for the design of flexural reinforcement of reinforced concrete walls. The correlation satisfactorily agrees with the experimental results when no premature failure of the strengthening composite material takes place.

6.2. Recommendations

Below is a series of recommendations for future tests that seek to continue with the study of external reinforcement of slender concrete walls with FRP bands.

- It is necessary to consider in future tests the influence that the axial load has on reinforcing with FRP bands of slender reinforced concrete walls to improve their bending capacities.
- It is important to study different anchoring systems for the reinforcement scheme studied in this project, to guarantee an adequate behavior of the reinforcement system during seismic events.

- It is recommended in the future to carry out a project that studies the behavior of walls reinforced with FRP bands arranged in both vertical and horizontal orientation, to assess its effect on bending and shear capacities at the same time of walls with reinforcement deficiencies in both directions.
- It is necessary to evaluate in future tests if one-sided strengthening produces a significant eccentricity effects compared to double-sided strengthening.

The results of the study presented in this document are part of an ongoing research project being conducted at in conjunction between the University of Miami and the Escuela Colombiana de Ingeniería Julio Garavito.

BIBLIOGRAPHY

ACI 318. (2019). *Building Code Requirements for Structural Concrete*.

ACI 440.2R. (2017). 440.2R-17: Guide for the Design and Construction of Externally Bonded FRP Systems for Strengthening Concrete Structures. In *440.2R-17: Guide for the Design and Construction of Externally Bonded FRP Systems for Strengthening Concrete Structures*. https://doi.org/10.14359/51700867

Reglamento Colombiano de Construcción Sismo Resistente NSR-10, (2012).

Blandón, C. a, Fernando, J., & Ricardo, R. (2015). *Comportamiento de muros delgados de concreto reforzado ante cargas laterales Behavior of thin reinforced concrete walls under lateral load*. *May 2015*, 1–10.

Carrillo, Julian, Diaz, C., & Arteta, C. A. (2019). Tensile mechanical properties of the electro-welded wire meshes available in Bogotá Colombia. *Construction and Building Materials*, *195*, 352–362. https://doi.org/10.1016/j.conbuildmat.2018.11.096

Carrillo, Julián, Rico, A., & Alcocer, S. (2016). Experimental study on the mechanical properties of weldedwire meshes for concrete reinforcement in Mexico City. *Construction and Building Materials*, *127*.

CEER (Colombian Earthquake Engineering Research Network). (2018). *Estudio del Comportamiento Sísmico de Edificios de Muros Delgados de Concreto Reforzado* (Issue 002).

Correal, J. F. (2016, April 23). ¿Cuán vulnerable es Colombia ante un sismo? *El Tiempo*. https://www.eltiempo.com/archivo/documento/CMS-16571309

Cruz-Noguez, C. A., Lau, D. T., Sherwood, E. G., Hiotakis, S., Lombard, J., Foo, S., & Cheung, M. (2015). Seismic behavior of RC shear walls strengthened for in-plane bending using externally bonded FRP sheets. *Journal of Composites for Construction*, *19*(1), 1–10. https://doi.org/10.1061/(ASCE)CC.1943-5614.0000478

Di Luccio, G., Michel, L., Ferrier, E., & Martinelli, E. (2017). Seismic retrofitting of RC walls externally strengthened by flax–FRP strips. *Composites Part B: Engineering*, *127*, 133–149. https://doi.org/10.1016/j.compositesb.2017.06.017

El-Sokkary, H., & Galal, K. (2013). Seismic Behavior of RC Shear Walls Strengthened with Fiber-Reinforced Polymer. *Journal of Composites for Construction*, *17*(5), 603–613. https://doi.org/10.1061/(asce)cc.1943-5614.0000364

García R., L. E. (1998). *Dinámica estructural aplicada al diseño sísmico*. Universidad

de los Andes.

Hiotakis, S., Lau, D. T., & Londono, N. (2004). Research on seismic retrofit and rehabilitation of reinforced concrete shear walls using frp materials. *Concrete*.

ICRI 310.2R. (2013). *ICRI Guideline No. 310.2R-2013: Selecting and Specifying Concrete Surface Preparation for Sealers, Coatings, Polymer Overlays, and Concrete Repair. 310*.

Ko, H., & Sato, Y. (2008). Bond Stress – Slip Relationship between FRP Sheet. *Journal of Composites for Construction*, *11*(4), 419–426.

Lombard, J., Lau, D., & Humar, J. (2000). Seismic strengthening and repair of reinforced concrete shear walls. *Proc., 12th World Conf. on …*, 1–8. http://www.iitk.ac.in/nicee/wcee/article/2032.pdf

Nakaba, K., Kanakubo, T., Furuta, T., & Yoshizawa, H. (2001). Bond behavior between fiber-reinforced polymer laminates and concrete. *ACI Structural Journal*, *98*(3), 359–367. https://doi.org/10.14359/10224

Panneton, M., Léger, P., & Tremblay, R. (2006). Inelastic analysis of a reinforced concrete shear wall building according to the National Building Code of Canada 2005. *Canadian Journal of Civil Engineering*, *33*(7), 854–871. https://doi.org/10.1139/L06-026

Paulay, T., & Priestley, M. . (1992). *Seismic design of reinforced concrete and masonry buildings*.

Portafolio. (2019). Estas son las ciudades más pobladas del país, según el censo del Dane. *Portafolio*. https://www.portafolio.co/economia/estas-son-las-ciudades-mas-pobladas-del-pais-segun-el-censo-del-dane-534662

Qazi, S., Michel, L., & Ferrier, E. (2013). Mechanical behaviour of slender RC walls under seismic loading strengthened with externally bonded CFRP. *European Journal of Environmental and Civil Engineering*, *17*(6), 496–506. https://doi.org/10.1080/19648189.2013.791076

Rousakis, T. (2014). Encyclopedia of Earthquake Engineering. *Encyclopedia of Earthquake Engineering*, 1–15. https://doi.org/10.1007/978-3-642-36197-5

San Bartolomé, A., Muñoz, A., Villagarcía, M., & Acuña, C. (2007). *Comportamiento Sísmico De Placas De Concreto Reforzadas Con Mallas Electrosoldadas*. 1–15.

San Bartolome, A., Quiun, D., & Silva, W. (2011). Comentarios Relativos Al Tipo De Falla En Los Muros De Concreto De Edificios Chilenos En El Sismo Del 27 De Febrero De 2010. *Concreto y Cemento. Investigación y Desarrollo*, *3*(1), 36–48.

Sheikh, S. A., Derose, D., & Mardukhi, J. (2002). *99-S47.Pdf*. *99*, 451–459.

Shen, D., Yang, Q., Jiao, Y., Cui, Z., & Zhang, J. (2017). Experimental investigations on reinforced concrete shear walls strengthened with basalt fiber-reinforced polymers under cyclic load. *Construction and Building Materials*, *136*(October 2018), 217–229. https://doi.org/10.1016/j.conbuildmat.2016.12.102

Siddika, A., Mamun, M. A. Al, Ferdous, W., & Alyousef, R. (2020). Performances, challenges and opportunities in strengthening reinforced concrete structures by using FRPs – A state-of-the-art review. *Engineering Failure Analysis*, *111*(August 2019), 104480. https://doi.org/10.1016/j.engfailanal.2020.104480

Teng, J. G., Chen, J. F., Smith, S. T., & Lam, L. (2003). Behaviour and strength of FRP-strengthened RC structures: A state-of-the-art review. *Proceedings of the Institution of Civil Engineers: Structures and Buildings*, *156*(1), 51–62. https://doi.org/10.1680/stbu.2003.156.1.51

Tumialan, G., Vatovec, M., & Kelley, P. (2009). FRP Composites for Mansory Retrofitting: Review of Engineering Issues, Limitations and Practical Applications. *Structure Magazine*.

Vega Vargas, C. J. (2015). *Comportamiento dinámico de muros de mampostería no estructural reforzados mediante polímeros reforzados con fibra de carbono, CFRP*.

A. Annex: Hysteresis Curves

Applied load versus mid-span displacement cycles for L-0 specimen.

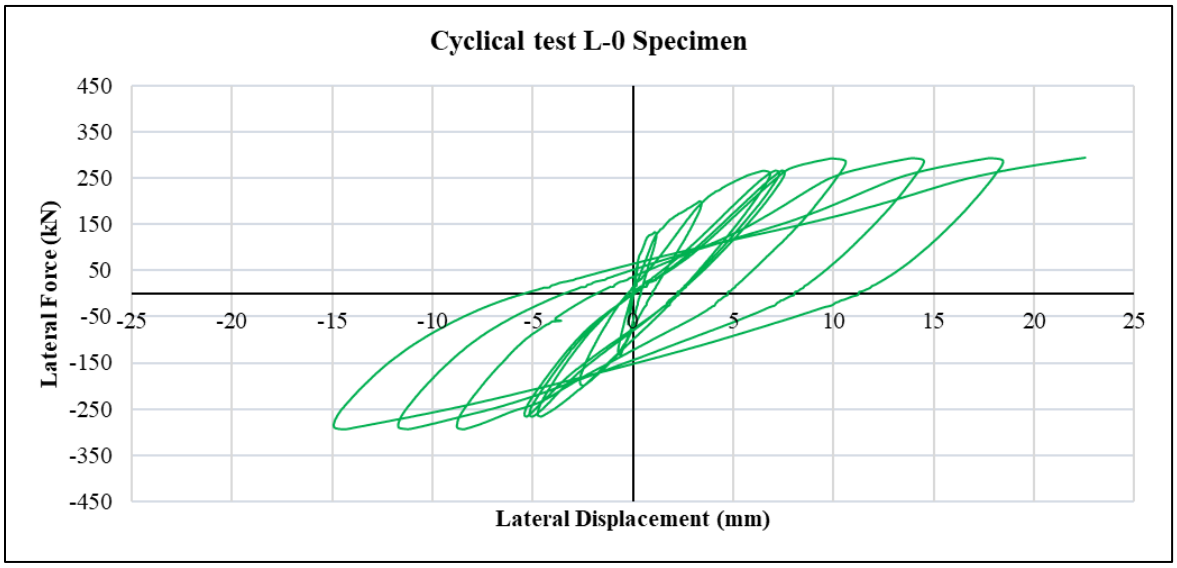

Applied load versus mid-span displacement cycles for L-GHS-1 specimen.

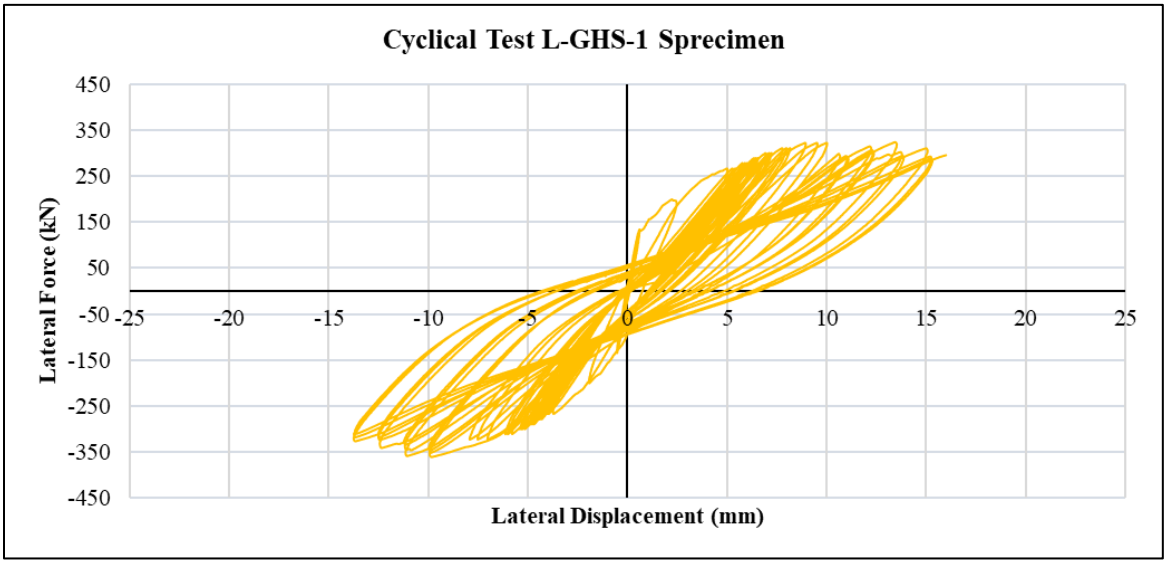

Applied load versus mid-span displacement cycles for L-CHS-1 specimen.

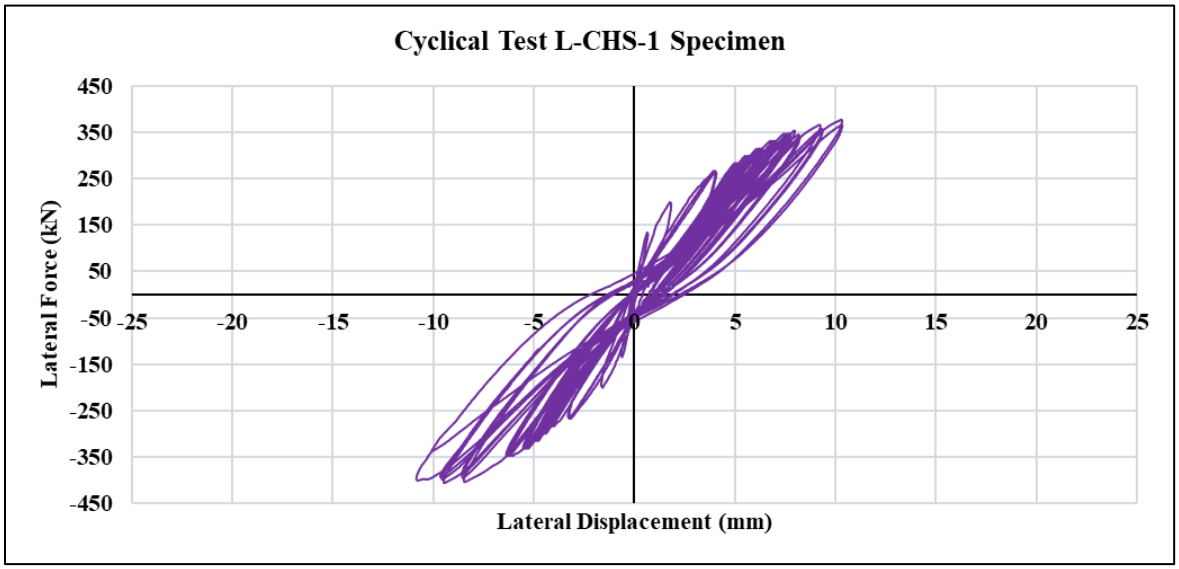

Applied load versus mid-span displacement cycles for L-CHS-2 specimen.

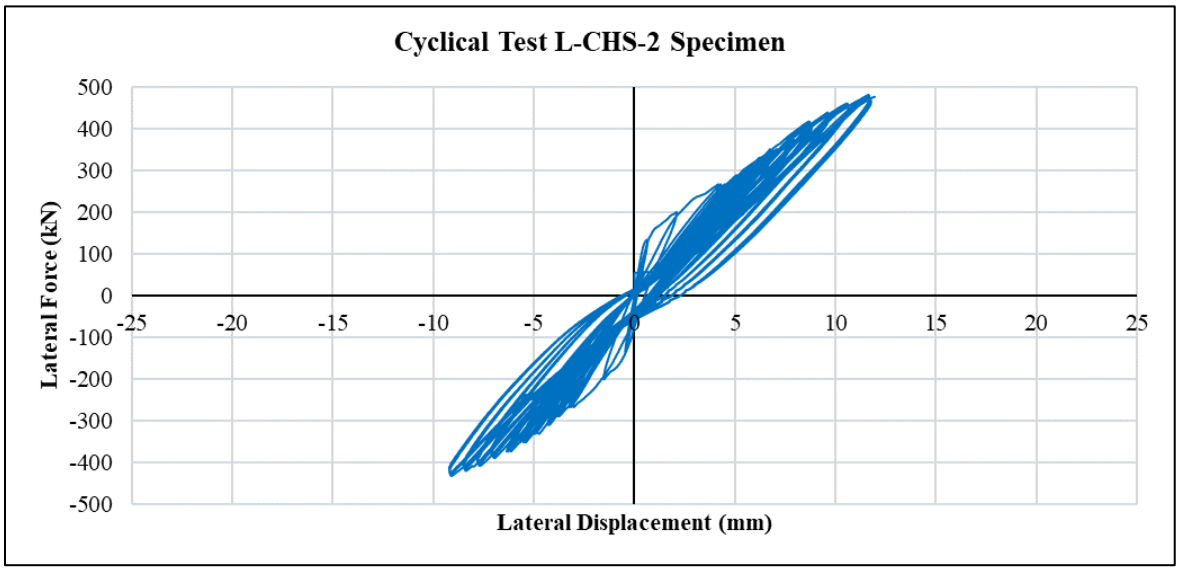

Applied load versus mid-span displacement cycles for H-0 specimen.

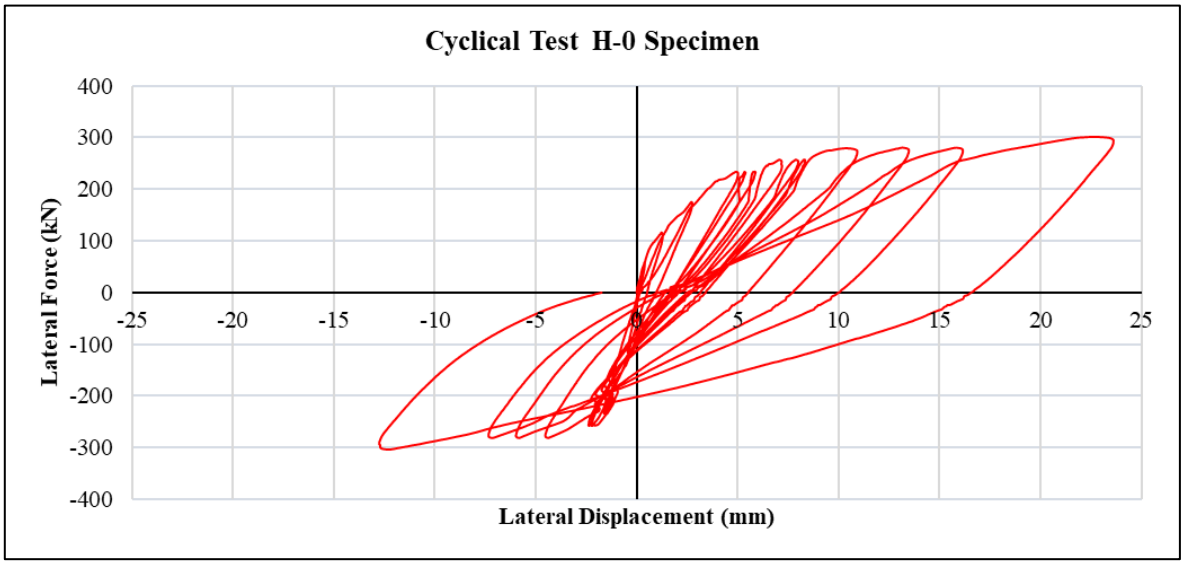

Applied load versus mid-span displacement cycles for H-0 specimen.

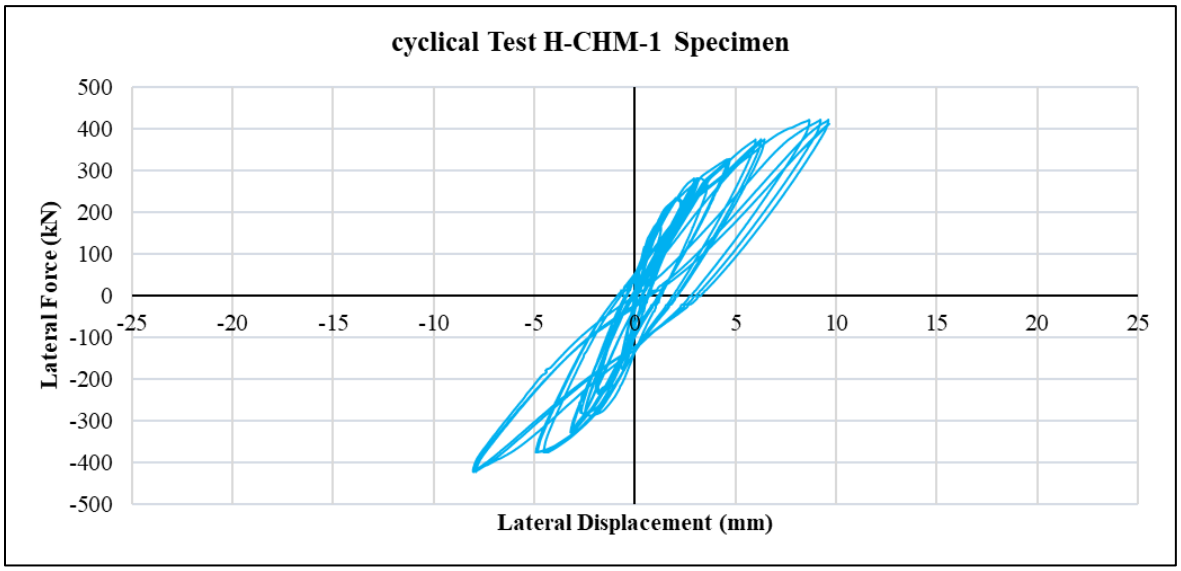

B. Annex: FRP reinforcement design

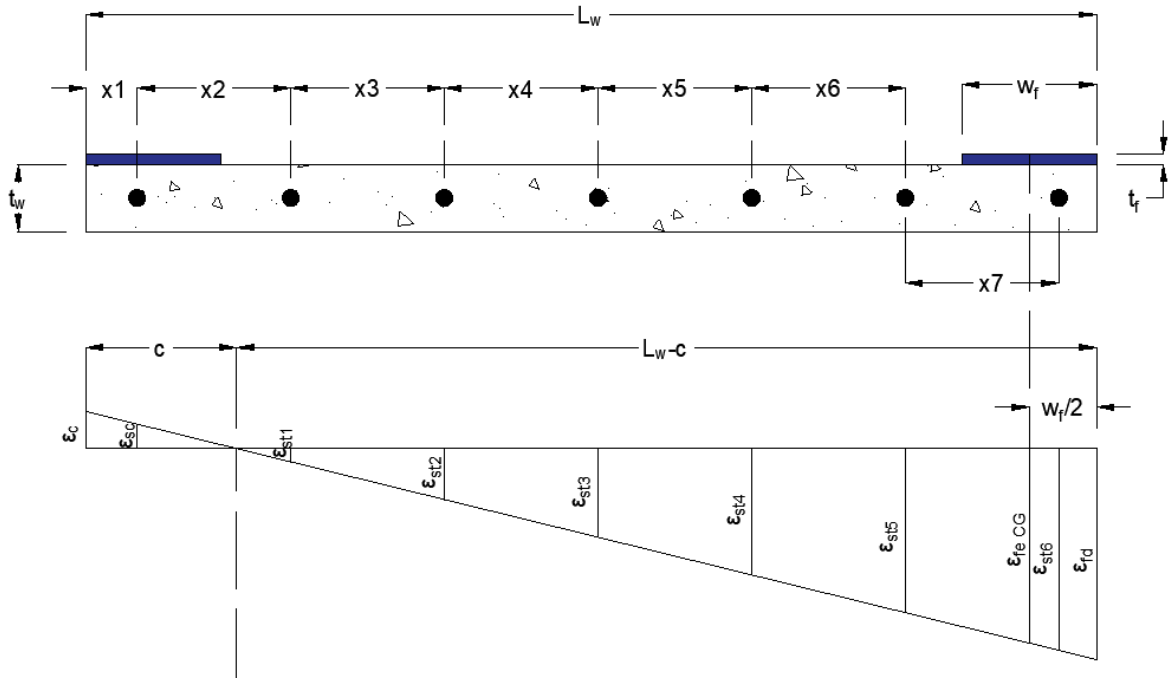

L-GHS-1

As built shear wall properties and demands		
Concrete strength, f´c=	24.1 MPa	3500 psi
Longitudinal reinforcing steel yield strength, fy=	450 MPa	65.3 ksi
Modulus of elasticity of steel, Es=	214286 MPa	31 071 ksi
Longitudinal reinforcing yield strain, εy=	0,0021 mm/mm	0.0021 in/in
Shear wall length, Lw=	1.5 m	59 in
Shear wall thickness, tw=	0.1 m	4 in
Number of layers, n=	1	1
FRP strips wide, wf=	200 mm	7.87 in
Existing wall reinforcement: **Horizontal: No. 4 at 6 in. (150 mm) on center** **Vertical: No.4 at 9 in. (229 mm) on center**		
Manufacturer´s reported composite properties		
Thickness per ply, tf=	1.016 mm	0.04 in
Ultimate tensile strength, ffu=	567 MPa	82 236 psi
Rupture strain, εfu=	0,0213 mm/mm	0.0213 in/in
Modulus of elasticity, Ef=	26 680 MPa	3 870 ksi

Compute the debonding strain limit, ε_{fd}:

$$\varepsilon_{fd} = 0.41\sqrt{\frac{f'c}{n \cdot E_f \cdot t_f}} = 0{,}01223\ mm/mm\ \leq 0{,}9 \cdot \varepsilon_{fu} = 0{,}01917\ mm/mm$$

FRP strips area, A_f:

$$A_f = t_f \cdot w_f = 203{,}2\ mm^2$$

Assume the depth of the neutral axis, c:

Assume that the effective strain is at the centroid of the FRP area. Knowing the maximum effective strain in the FRP, compute the force in the FRP:

$$T_f = A_f \cdot \varepsilon_{fd} \cdot E_f = 66.3\ kN$$

Assume that all steel bars in the wall yields, except for the one bar that is adjacent to the compression faces, the steel area in yield, A_{sw}:

$$A_{sw} = 6 \cdot A_{No.6\ bar} = 774\ mm^2$$

Depth of corresponding compression block, a:

$$a = \frac{A_{sw} \cdot f_y + T_f}{0.85 \cdot f'c \cdot t_w} = 202.4\ mm$$

Compute an estimate of the depth of the neutral axis, c:

$$c = \frac{a}{0.85} = 238.1\ mm$$

Check actual strain at centroid of FRP area and corresponding force in the FRP:

$$\varepsilon_{feCG} = \varepsilon_{fd} \cdot \left(1 + \frac{{}^{w_f}/_2}{c - L_w}\right) = 0.01126\ mm/mm$$

$$T_f = A_f \cdot \varepsilon_{feCG} \cdot E_f = 61.0\ kN$$

It is observed that the force in the FRP does not agree with that based on the initial assumption. However, the above steps provide a reasonable starting point for an assumption for c= 238.1 mm.

Compute concrete strain at extreme compression surface, ε_c:

$$\varepsilon_c = \varepsilon_{fd} \cdot \left(\frac{c}{L_w}\right) = 0.0023\ mm/mm < \varepsilon_{cu} \qquad ok!!$$

Compute strain in the bar in the compression zone:

$$\varepsilon_{sc} = \left(\frac{\varepsilon_c}{c}\right) \cdot (c - X_1) = 0.0016\, mm/mm$$

Where X_1=76 mm.

Compute strain in the bars in the tension zone:

$$\varepsilon_{st1} = \left(\frac{\varepsilon_c}{c}\right) \cdot (c - X_1 - X_2 - X_3 - X_4 - X_5 - X_6 - X_7) = 0.0004\, mm/mm$$

Similarly:

$$\varepsilon_{st2} = 0.0026\, mm/mm$$

$$\varepsilon_{st3} = 0.0048\, mm/mm$$

$$\varepsilon_{st4} = 0.0071\, mm/mm$$

$$\varepsilon_{st5} = 0.0093\, mm/mm$$

$$\varepsilon_{st6} = 0.0115\, mm/mm$$

Compute strain at centroid of FRP area:

$$\varepsilon_{feCG} = 0.01126\, mm/mm$$

$$T_f = 61.0\ kN$$

Recompute total tensile force components at the above determined strain levels:

$$T_{sw} = 301.7\ kN$$

Recalculate depth of compression block and depth to neutral axis:

$$a = \frac{T_{sw} + T_f}{0.85 \cdot f'c \cdot t_w} = 177.1\, mm$$

$$c = \frac{a}{0.85} = 208.31\, mm$$

Final value of the depth of the neutral axis is achieved after iteration:

$$c = 212.15\, mm$$

$$\varepsilon_c = \varepsilon_{fd} \cdot \left(\frac{c}{L_w}\right) = 0.0020\, mm/mm < \varepsilon_{cu} \qquad ok!!$$

$$\varepsilon_{sc} = \left(\frac{\varepsilon_c}{c}\right) \cdot (c - X_1) = 0.0013\ mm/mm$$

Force in the bar in the compression zone:

$$C_{sc} = E_s \cdot \varepsilon_{sc} \cdot A_{No.4\ bar} = 35.7\ kN$$

Strains and forces in bars in tensile zone:

$$\varepsilon_{st1} = 0.0007\ mm/mm$$

$$\varepsilon_{st2} = 0.0028\ mm/mm$$

$$\varepsilon_{st3} = 0.0050\ mm/mm$$

$$\varepsilon_{st4} = 0.0072\ mm/mm$$

$$\varepsilon_{st5} = 0.0093\ mm/mm$$

$$\varepsilon_{st6} = 0.0115\ mm/mm$$

$$T_{sw} = 308.3\ kN$$

Strain and force in FRP:

$$\varepsilon_{feCG} = 0.01128\ mm/mm$$

$$T_f = 61.1\ kN$$

From equilibrium, compressive force in concrete:

$$C_c = T_{sw} + T_f + C_{sc} = 334\ kN$$

Calculate the moment capacity of the section:

Compute lever arm for different force components:

Arms for different force components:

Bar in compression=	-674	mm
Concrete compression=	-660	mm
First bar in tension=	-445	mm
Second bar in tension=	-217	mm
Third bar in tension=	0	mm
Fourth bar in tension=	217	mm
Fifth bar in tension=	445	mm
sixth bar in tension=	674	mm

Nominal moment capacity, M_n:

$$M_n = 340.9\ kN - m$$

Ultimate load at middle of the height:

$$P_n = \frac{M_n \cdot 4}{4.5\ m} = 303\ kN$$